Science of the Total Environment 950 (2024) 175277

Contents lists available at ScienceDirect

Science of the Total Environment

journal homepage: www.elsevier.com/locate/scitotenv

Shifting from traditional landslide occurrence modeling to scenario estimation with a "glass-box" machine learning

Francesco Caleca [a,*], Pierluigi Confuorto [a], Federico Raspini [a], Samuele Segoni [a], Veronica Tofani [a], Nicola Casagli [a,b], Sandro Moretti [a]

[a] Department of Earth Sciences, University of Florence, Florence, Italy
[b] National Institute of Oceanography and Applied Geophysics - OGS, Borgo Grotta Gigante, Sgonico, Trieste, Italy

HIGHLIGHTS

- A "glass-box" machine learning model is used to map landslide susceptibility under extreme rainfall event conditions
- A new rainfall variable, namely rainfall anomaly, expresses the intensity of the event compared to past rainfall patterns
- Rainfall anomaly and model intelligibility are used to estimate landslide occurrence under different rainfall scenarios

GRAPHICAL ABSTRACT

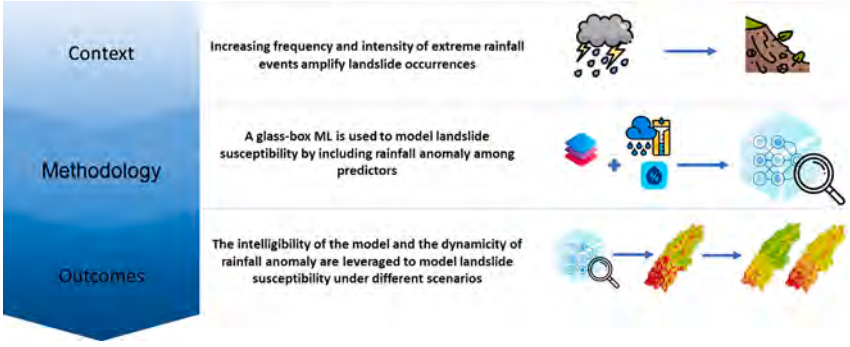

ARTICLE INFO

Editor: Fernando Pacheco

Keywords:
Landslides
Machine-learning
Glass-box models
Landslide susceptibility
EBMs
Extreme rainfall events
Italy

ABSTRACT

Extreme rainfall events represent one of the main triggers of landslides. As climate change continues to reshape global weather patterns, the frequency and intensity of such events are increasing, amplifying landslide occurrences and associated threats to communities. In this contribution, we analyze relationships between landslide occurrence and extreme rainfall events by using a "glass-box" machine learning model, namely Explainable Boosting Machine. What sets these models as a "glass-box" technique is their exact intelligibility, offering transparent explanations for their predictions. We leverage these capabilities to model the landslide occurrence induced by an extreme rainfall event in the form of spatial probability (i.e., susceptibility). In doing so, we use the heavy rainfall event in the Misa River Basin (Central Italy) on September 15, 2022. Notably, we introduce a rainfall anomaly among our set of predictors to express the intensity of the event compared to past rainfall patterns. Spatial variable selection and model evaluation through random and spatial routines are incorporated into our protocol. Our findings highlight the critical role of the rainfall anomaly as the most important variable in modeling landslide susceptibility. Furthermore, we leverage the dynamic nature of such a variable to estimate landslide occurrence under different rainfall scenarios.

* Corresponding author.
E-mail address: francesco.caleca@unifi.it (F. Caleca).

https://doi.org/10.1016/j.scitotenv.2024.175277
Received 30 May 2024; Received in revised form 19 July 2024; Accepted 2 August 2024
Available online 8 August 2024

1. Introduction

Landslides induced by extreme rainfall events represent a significant threat to communities in many regions around the world (Clò et al., 2024; Haque et al., 2019; Kirschbaum et al., 2012; Marengo et al., 2020). These events occur when heavy rainfalls exceed the drainage capacity of soils, leading to unstable conditions. As a result, mass movements are mainly triggered due to an increase in pore-pressure, and an associated decrease in soil strength (Bogaard and Greco, 2016; Wang and Sassa, 2003). Extreme rainfall events are often associated with weather phenomena such as tropical cyclones, monsoons, or intense convective storms (Barlow et al., 2019; Dayan et al., 2015; Prein et al., 2017). As climate change continues to influence global weather patterns, the frequency and intensity of these events are expected to increase, amplifying the probability of landslide occurrence (Crozier, 2010; Gariano and Guzzetti, 2016). This implies an increasing threat for communities residing in landslide-prone areas.

Understanding and modeling the occurrence of such events is a crucial step in implementing landslide risk assessments (Corominas et al., 2014) or suitable early warning systems (Intrieri et al., 2012). Forecasting "where" a landslide might occur belongs to the landslide susceptibility framework (Guzzetti, 2005). The term landslide susceptibility refers to the likelihood of a landslide or a population of landslides in a given area based on the terrain conditions (Brabb, 1984). Oftentimes, landslide susceptibility is confused with landslide hazard (Reichenbach et al., 2018). However, it is important to stress that susceptibility represents only the spatial component of hazard assessment (Caleca et al., 2022; Guzzetti et al., 2005).

Since the 1970s, research on landslide susceptibility has yielded a variety of approaches, broadly classified into the following categories: i) analysis of landslide inventories (Campbell, 1973; Carrara and Merenda, 1976; Wieczorek, 1984); ii) geomorphological mapping (Lee, 2001; Pike, 1988; Reichenbach et al., 2005); iii) knowledge-driven or heuristic methods (Barredo et al., 2000; Hansen et al., 1995; Stanley and Kirschbaum, 2017); iv) physically-based models (Alvioli et al., 2014; Montgomery and Dietrich, 1994; Rossi et al., 2013; Salvatici et al., 2018); v) statistically-based models (Carrara et al., 1991; Lombardo and Mai, 2018; Reichenbach et al., 2018; Yalcin, 2008; Zêzere et al., 2017). The initial three categories, marked by an inherent subjectivity, are largely superseded by physical and statistically-based approaches in the last decades.

Statistically-based models belong to the family of data-driven approaches (Lima et al., 2022). They are based on the assumption that past landslide occurrences might be the key to predicting new ones (Corominas et al., 2014). This implies that a data-driven model is capable of analyzing the relationship between the distribution of stable/unstable slopes with a set of predisposing/triggering factors (Guzzetti et al., 2012). Specifically, the target distribution represents the dependent variable of the model and is typically expressed in a binary structure (i.e., presence or absence of landslides) within the selected mapping unit, either a regular grid (Meijerink, 1988) or a slope unit (Carrara et al., 1991; Giles and Franklin, 1998). As a consequence, the fitted model is adopted to define the propensity of landsliding for each mapping unit. The field of statistically-based models has seen the growth of different techniques, spanning from linear models (Camilo et al., 2017) to recent deep learning approaches (Huang et al., 2020). Generalized Linear Models (GLMs) (Nelder and Wedderburn, 1972) represent one of the most common approaches in landslide susceptibility modeling (Ayalew and Yamagishi, 2005; Lee, 2005; Lombardo and Mai, 2018; Merghadi et al., 2020; Steger et al., 2017). The main advantage of GLMs is the clear interpretability, stemming from their treatment of the effect of covariates on the landslide event as a linear function. However, this assumption may be a simplification of these relationships and may not hold for all factors (Brenning et al., 2015). In view of this, alternative approaches have been implemented, aiming to incorporate non-linear effects and capture more complex relationship between landslide occurrence and triggering/predisposing factors. Among the alternatives, Generalized Additive Models (GAMs) have earned attention for their capacity to improve flexibility through the incorporation of smooth functions (Hastie and Tibshirani, 1987), thereby allowing non-linear relationships (Brenning, 2008; Goetz et al., 2011; Lin et al., 2021). Other notable approaches are decision tree models (Arabameri et al., 2022; Nefeslioglu et al., 2010) and Random Forest algorithms (Catani et al., 2013; Rosi et al., 2023; D. Sun et al., 2020; Zhang et al., 2023), which demonstrate efficacy in capturing complex non-linear patterns. Support Vector Machines (SVMs) (Huang and Zhao, 2018; Yao et al., 2008) constitute another facet of alternative approaches. Furthermore, Artificial Neural Networks (ANNs) (Amato et al., 2023; Ermini et al., 2005; Gameiro et al., 2021) and Deep Learning approaches (Azarafza et al., 2021; Bui et al., 2020; Van Dao et al., 2020; Xia et al., 2024), represent a category of models that exhibits notable efficacy in capturing intricate relationships.

Aside from GAMs, which still allow the visualization and associated interpretation of how predictors affect the response variable, recent machine-learning techniques direct their efforts towards higher predictive capabilities at the expense of interpretability (Caruana et al., 2020; Murdoch et al., 2019). In other words, simpler models like GLMs are easier to interpret, while complex models like deep neural networks are harder to interpret (Baryannis et al., 2019; Greenwell et al., 2023; Linardatos et al., 2020). For this reason, complex algorithms are commonly named "black-box" models (Rudin, 2019).

In the context of modeling landslide occurrence, the ability to provide high-accurate results accompanied by explainable predictions represents a valuable tool. In light of this consideration, Dahal and Lombardo (2023) showcase the potential of Explainable Artificial Intelligence (ExAI) in landslide susceptibility modeling. Recently, the geoscience community has been shifting towards the adoption of more interpretable algorithms (Collini et al., 2022; Toms et al., 2020; Youssef et al., 2023). This trend arises from the wish to unravel the intricate mechanisms behind predictive models, making them not only high-performing but also comprehensible to any user.

In this contribution, we model the landslide occurrence in the form of susceptibility by exploring the capabilities of a recent generation of interpretable models, namely Explainable Boosting Machines (hereafter EBMs) (Nori et al., 2019). Unlike the majority of explainable approaches that unveil the decisions of a "black-box" model in a post-processing step using techniques like SHAP (SHapley Additive exPlanations) (Lundberg and Lee, 2017), LIME (Local Interpretable Model-agnostic Explanations) (Ribeiro et al., 2016), or sensitivity analyses for the impact of each variable on predictions (Jacinth Jennifer and Saravanan, 2021), EBMs offer direct interpretability. This implies that the generated explanations are exact, providing full transparency. As a consequence, EBMs fall into the category of "glass-box" models. Despite their potential implications in landslide susceptibility modeling, EBMs have rarely been employed in this field. A careful review of the literature shows only one instance of their application in such studies, described by Maxwell et al. (2021). Given this gap, we aim to explore and demonstrate their capabilities in landslide susceptibility modeling.

Specifically, the incorporation of "glass-box" models within studies focusing on the relationship between landslide occurrence and extreme rainfall events raises considerable interest and represents the aim of this study. To do so, we use as context the landslides occurrence triggered by a heavy rainfall event on September 15, 2022, in the Misa River basin (Central Italy). To analyze the interaction between slope failure and the event, we include a rainfall anomaly among our set of predictors, which expresses the intensity of such an event compared to the average annual cumulative rainfall. Notably, this variable is computed as the percentage of precipitation attributed to the event compared to the mean annual rainfall.

To summarize (see Fig. 1), we implement an EBM for modeling landslide susceptibility by including a spatial variable selection scheme for identifying the optimal subset of predictors. The predictive

capabilities of the model are evaluated through two different cross-validation routines. The outcomes identify the areas more prone to failure, highlighting the paramount role of rainfall anomaly in defining the spatial pattern of triggered landslides. Notably, the fitted model might be also useful in predicting new unstable areas under different weather conditions and rainfall events by leveraging the dynamic nature of rainfall anomaly variable. This might represent a useful tool for land use planning and risk mitigation in the context of climate change and the expected increased frequency of extreme events.

2. Study area and landslide inventory

The geographic context we leverage as a study area is the Misa River basin (Central Italy – Marche region), which is a part of the Northern Marchean Apennines. From a geological perspective, hemipelagic, turbiditic and evaporitic deposits from the Miocene to lower Pleistocene overly a Jurassic-Paleogene carbonate succession (Calderoni et al., 2010; Vannoli et al., 2004). The most recent tectonic phase (Upper Pliocene – Lower Pleistocene) caused the emersion of the piedmont area (Bartolini, 2003; Centamore et al., 1996; Seta et al., 2008) with the contemporary establishment of the first stream network (Mayer et al., 2003). As a consequence of this phase, the main watercourses are southwest-northeast oriented.

The Misa River basin covers an area of approximately 384 km^2, ranging from a maximum elevation of 825 m above sea level to a minimum elevation equal to sea level (Fig. 2A). From a geomorphological point of view, the Misa River basin can be split into two main parts: i) a mountainous region with steep slopes situated in the southwestern sector, characterized by the presence of marly limestone and flysch formations from the Apennine chain (Centamore et al., 1979; Coltori, 1997); ii) in the northeastern part, a flatter piedmont sector that extends towards the Adriatic sea. Here, the river valley is characterized by fluvial terraces, showcasing alluvial and eluvial-detrital sediments resulting from river transport (Coltori, 1997).

On September 15, 2022, the region was subjected to an unprecedented rainfall event. Gauge stations distributed across the study area recorded a maximum precipitation of 204 mm within 12 h. Moreover, few stations in the proximity of the study area reported a rainfall amount of 480 mm in only 9 h. The event's intensity triggered widespread landslides and floods, which caused extensive damage and human life losses. The extreme severity of the impacts is testified by the activation of a national-level state of emergency, which is a relatively uncommon measure, especially if compared with other parts of Italy (Gatto et al., 2023). Specifically, 630 shallow landslides have been mapped within the Misa River basin. Their mapping has been realized through visual interpretation with the support of semi-automated methods implemented on Very High Resolution optical multispectral images, validated and integrated with in situ survey carried out in the aftermath of the 15 September event. The acquired optical images consist of several datasets, whose spatial resolutions range from 0.4 m to 3 m. Looking at the spatial distribution of landslides (Fig. 2A), reveals a notable concentration in the mountainous sector, with only a few instances occurring in the flatter area. In the mountainous area, landslides have been triggered on sandy and calcareous soils with high permeability. On the contrary, hilly and flatter areas are mainly characterized by clay soils with low permeability overlaid by eluvial deposits. According to the World Reference Base for Soil Resource classification (Deckers and Nachtergaele, 1998), the most prevalent soil families are calcaric regosols and calcisols. Specifically, these latter are present with varying calcium carbonate concentrations, including categories such as hypercalcic and hypocalcic. The occurrence of landslides in these gently sloping areas underscores the extraordinary nature of the event, emphasizing its capacity to generate such phenomena even in less steep terrain.

3. Data and methods

In the following sections, we describe the mapping unit for our modeling purposes (Section 3.1), the predisposing and triggering factors

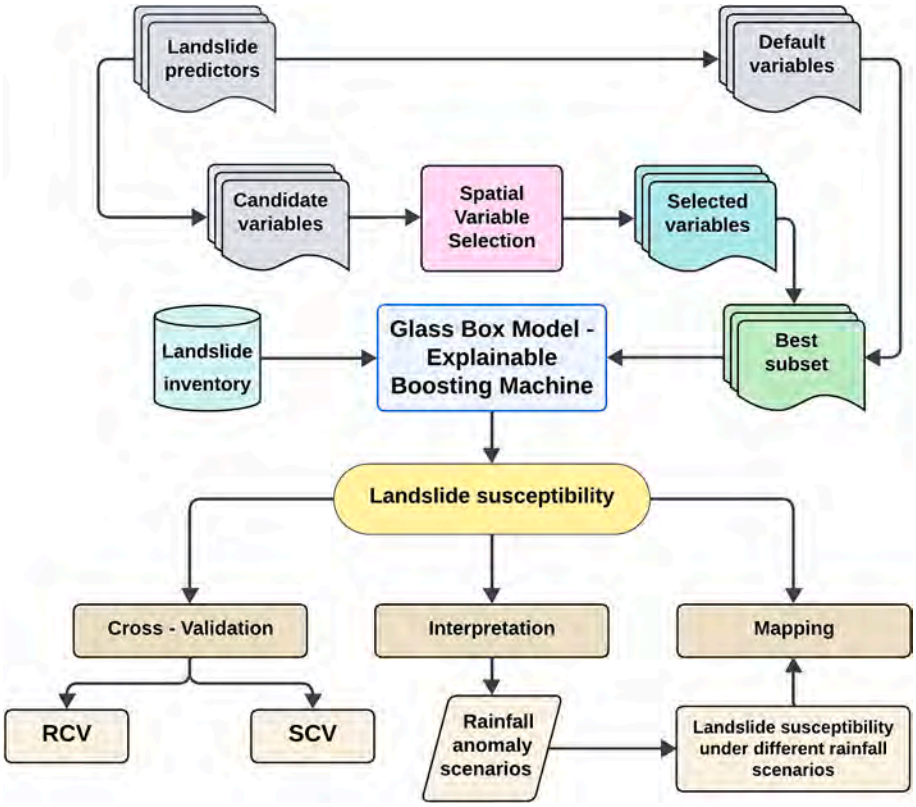

Fig. 1. Flowchart of the methodological phases in this work.

we include in our set of landslide predictors (Section 3.2) as well as the structure of the model (Sections 3.3 and 3.3.1) and the routines we implement for evaluating its performance (Section 3.4).

3.1. Mapping unit

In this contribution, we divide our study area into Slope Units (hereafter SUs). A SU is a topographical unit defined by hydrological and geomorphological criteria and bounded by drainage and divide lines (Carrara et al., 1991; Carrara, 1983; Giles and Franklin, 1998; Tsukamoto and Ohta, 1988). Although no universally accepted cartographic unit exists as the optimal choice for landslide susceptibility modeling (Ba et al., 2018; Erener and Düzgün, 2012), the concept of SUs aligns well with the depiction of single slopes, a combination of adjacent slopes, or sub-catchments. This implies that SU-based models are highly reliable from a geomorphological perspective, thereby supporting their suitability for such applications (Chang et al., 2023; Guzzetti et al., 2006, 1999; Jacobs et al., 2020; Loche et al., 2022; Lombardo et al., 2020).

The partition is done by using the *r.slopeunits* software developed by Alvioli et al. (2016). The software automatically delineates SUs requiring as only input data a Digital Elevation Model (DEM). SUs are generated by clustering pixels of slope exposure and following hydrological criteria. This relies on a set of parameters that users are required to configure. For a detailed technical description of these parameters, we refer the reader to Alvioli et al. (2016). The configuration we adopt is reported below: minimum area = 15,000 m^2; circular variance = 0.4; clean size = 10,000 m^2; threshold = 20,000 m^2; reduction factor = 10.

The partition is built upon a 10 × 10 m DEM (Tarquini et al., 2023, 2007) and results in 2049 SUs (Fig. 2B) with a mean planimetric area of 0.20 km^2 and a variability of 0.19 km^2 expressed into a single standard deviation. Each of the generated SUs represents the target of the modeling we implement.

3.2. Landslide predictors

The variables to be included in the set of landslide predictors should contain information to be statistically related to the observed landslide presence or absence in each mapping unit (Budimir et al., 2015; Glade and Crozier, 2005; Guzzetti, 2005; Lima et al., 2023). For our modeling, we create an initial set of eighteen environmental and terrain variables including geomorphological, geological, land-use, soil and meteorological properties. Specifically, predisposing and triggering factors are selected according to current literature (Conforti and Ietto, 2021; Liu et al., 2023; Reichenbach et al., 2018), the availability and quality of data as well as the knowledge of characteristics of the study area and the type of landslides under investigation.

The geomorphological parameters are derived from a 10 × 10 DEM (Tarquini et al., 2023, 2007), and include: i) slope steepness (Taylor, 1948; Zevenbergen and Thorne, 1987); ii) general, profile and planar curvature (Heerdegen and Beran, 1982; Moore et al., 1991); iii) eastness and northness (Brenning and Trombotto, 2006; Stage, 1976); iv) Topographic Wetness Index (Beven and Kirkby, 1979; Moore et al., 1991); v) Stream Power Index (Moore et al., 1991); vi) upslope contributing area and catchment slope angle (Quinn et al., 1991). Notably, we opt to include the upslope contributing area, transformed logarithmically to reduce skewness, and its average slope angle (catchment slope angle), as proxy for soil moisture and depth, and destabilizing forces upslope (see, Brenning et al., 2015; Persichillo et al., 2017).

The geological property is represented by the outcropping lithology in the study area and is extracted by a national lithological map of Italy (see, Bucci et al., 2022). The land-use component is expressed through the land-cover distribution and acquired from the 2018 version of CORINE-Land Cover database (Bossard et al., 2000). The information on soil properties is represented by the spatial distribution of soil typologies across the study area, and related data are accessed through a regional database (http://suoli.regione.marche.it/ServiziInformativi/Cartografia.aspx).

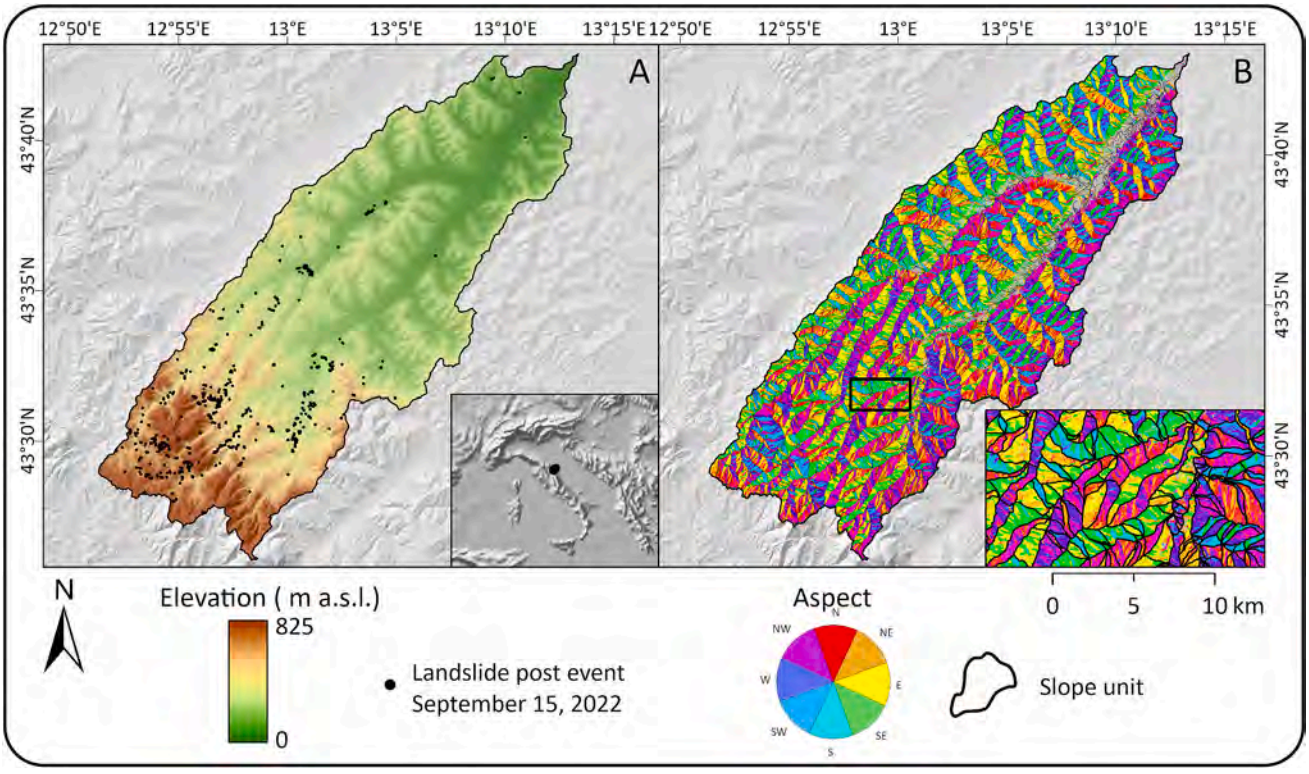

Fig. 2. Panel A depicts the elevation of the study area and the locations of landslides triggered on September 15, 2022. In Panel B, the partition of slope units and the exposition of slopes in the study area are illustrated.

To capture the meteorological forcing, we opt to include two different variables, respectively rainfall anomaly and preparatory rainfall. Rainfall anomaly is designed to convey the magnitude of the rainfall event on September 15, 2022, in comparison to annual rainfall patterns. To do so, we collected rainfall data records for both the target event and each year, starting from 2009, which is the common initial recording year for all gauge stations within the study area. Subsequently, we compute both the cumulative 24-h rainfall of the event and the mean annual rainfall for each station over the period spanning from 2009 to 2021. In turn, we define a rainfall anomaly for each station. This is achieved by dividing the respective cumulative 24-h precipitation and mean annual rainfall. As a result, we obtain the percentage of precipitation attributed to the September 15, 2022 event relative to the mean annual rainfall for each station. For instance, a hypothetical value of 0.15 means that at the specific location, the recorded rainfall measured during the event amounted to 15% of the mean annual rainfall. To spatially distribute the acquired rainfall anomalies from the local rain gauge network to the total extent of the study area, we interpolate such values by using the *Inverse Distance Weighted* (IDW) technique (Philip and Watson, 1982; Watson, 1985). The preparatory rainfall expresses the cumulative precipitation over the 30 days leading up to the occurrence on September 15, 2022. This antecedent rainfall serves as an indicator to assess the contribution of antecedent rainfall as a preparatory factor to predispose landslide triggering during the event. Equally to the rainfall anomaly computation, the preparatory variable is computed for all rain gauges and then spatially interpolated through the IDW algorithm.

In addition to all the described predictors, we incorporate two more variables: the slope unit area and catchment ID. Despite these parameters do not describe any predisposing or triggering condition, they are included for modeling purposes. Specifically, the slope unit area is considered to account for a bias that may arise from a spatial uneven landslide mapping (Loche et al., 2022; Steger et al., 2017; Steger et al., 2016a, 2016b). SUs with a larger area might contribute much more to the final probability of landslide occurrence compared to ones with a smaller extent (see, Moreno et al., 2024). The catchment ID is designed to induce a spatial proximity dependence in our model. Notably, a spatial model requires that mapping units located close to each other should be treated differently to those far from them (see, Wang et al., 2024b).

Dealing with a SU-based model requires choosing an attribute to describe the variability of predictors within SUs. The most common approach is to express their distribution by assigning for each SU the mean and standard deviation of each variable (Canavesi et al., 2020; Lombardo et al., 2021; Schlögel et al., 2018; X. Sun et al., 2020). An alternative strategy is to express the variability by accounting for the quantile values (Amato et al., 2019; Camilo et al., 2017). In this work, we opt to represent the distribution of continuous variables through the mean and standard deviation values.

To summarize this information, we list the predictors and their respective statistical attributes in Table 1.

Table 1
Predictor summary table. Continuous variables are aggregated to SU-level by calculating their respective mean or standard deviation values. Categorical variables are included by defining the predominant class. Each statistical attribute indicates a single predictor.

Predictor	Statistical attribute
Slope steepness	Mean and standard deviation
General curvature	Mean
Planar curvature	Mean
Profile curvature	Mean
Northness	Mean
Eastness	Mean
TWI	Mean
SPI	Mean
Contributing area	Mean
Catchment slope angle	Mean
Lithology	Majority
Land-cover	Majority
Soil type	Majority
Rainfall anomaly	Mean
Preparatory rainfall	Mean
Slope unit area	n.a.
Catchment ID	Majority

3.3. Model - explainable boosting machines

Explainable Boosting Machines (EBMs) are a new generation of Generalized Additive Models (GAMs), which offer both direct interpretability and competitive accuracy. Differently from GAMs, where non-linear relationships between dependent variable and independent variables are accommodated using smoothing functions in the form of splines (Hastie and Tibshirani, 1987), EMBs use gradient boosting and decision trees (Nori et al., 2019). What distinguishes an EBM as a "glass-box" model is its straightforward intelligibility and not an approximation as in "black-box" explanation methods such as SHAP (see, Lundberg and Lee, 2017) or LIME (see, Ribeiro et al., 2016). In the context of our modeling, where the dependent variable indicates the presence or absence of landslides for each SU, we implement a Binomial EBM, whose general form can be expressed as follows:

$$log(odds(p)) = \beta_0 + \sum f_i(x_i) + \sum f_{i,j}(x_i, x_j), \quad (1)$$

where the term $log(odds(p))$ is the logarithm of the odds (i.e., logit link function) of landslide occurrence (p) that EBM models and it corresponds to:

$$log(odds(p)) = log\left(\frac{p}{1-p}\right), \quad (2)$$

In Eq. (1), β_0 stands for the global intercept of the model. Notably, an EBM learns each feature function $f_i(x_i)$ via a boosting procedure (Lou et al., 2012), which is restricted to train on one feature at a time in a round-robin cycle using a very low learning rate so that feature order does not matter (Nori et al., 2019). As a result, the final function (i.e., shape function) for each feature x_i is obtained by adding all the functions for that feature:

$$f_i(x_i) = f_i(x_i^1) + f_i(x_i^2) + f_i(x_i^3) + \ldots + f_i(x_i^r), \quad (3)$$

where r indicates the number of iterations. Such a procedure mitigates the effects of co-linearity among predictors and allows showing how each of them contributes to the model's prediction (Nori et al., 2019; Wick et al., 2020). This implies that each contribution can be visualized and understood by plotting f_i making EBMs highly intelligible. EBMs adopt the additive structure inherited from GAMs, enabling each independent variable to contribute to predictions in a modular fashion. This characteristic facilitates a straightforward understanding of how each feature influences the prediction (Nori et al., 2019).

The novelties introduced by EBMs also extend to the incorporation of two-dimensional interactions between variables, which further increases accuracy while maintaining intelligibility. In Eq. (1), this joint effect is captured by the term $f_{i,j}(x_i, x_j)$. Specifically, EBMs define the pairwise interaction effect of x_i and x_j using the FAST algorithm, for whose technical description we refer the reader to Lou et al. (2013). In our context, we leverage this skill of EBMs to model the interaction between the two precipitation parameters we include in our predictors: rainfall anomaly and preparatory rainfall.

Moreover, EBMs provide a means to quantify the overall importance of each independent variable in the model's prediction. To elaborate, EBMs take instances of a particular variable, pass them into the learned shape function, and compute the average of the absolute values across all data instances. This process can be expressed mathematically as follows:

$$y_{x_i} = \frac{\sum_{k=0}^{N} |f_i(x_{k,i})|}{N}, \quad (4)$$

where y_{x_i} is the absolute score (i.e., importance) of the feature x_i, k is the data instances, N is the number of data instances.

Similarly to "black-box" explanation methods (Dahal and Lombardo, 2023; Lundberg and Lee, 2017; Ribeiro et al., 2016), EBMs offer the capability to analyze the decision-making process for an individual prediction. This involves each function f_j serving as a lookup table for each predictor, providing a term contribution. These term contributions are added up, and passed through the link function, in our case the logarithm of the odds, to compute the final prediction.

As discussed in Section 3.2, we want to incorporate a mechanism in our modeling to avoid the propagation of a spatial bias that might arise from uneven landslide mapping. To do so, we leverage the flexibility that EBMs inherit from GAMs and use specific covariates (e.g., slope unit area) to capture the effect of such a bias during the model fit. In turn, we zero out the effects of such covariates during the prediction (Lin et al., 2021; Moreno et al., 2024; Steger et al., 2016a). As a result, the final output would remain unbiased (Steger et al., 2021).

The implementation of our EBM is accomplished in a *Python* environment (Van Rossum et al., 1995; Van Rossum and Drake, 2009) by using the *Interpret* library (Nori et al., 2019).

3.3.1. Spatial variable selection

Variable selection is a common procedure aiming to identify an optimal subset of predictors for constructing a model. Various techniques, such as Ridge (Hoerl and Kennard, 1970; McDonald, 2009), LASSO (Muthukrishnan and Rohini, 2016; Tibshirani, 1996), and stepwise approaches (Bendel and Afifi, 1977; Blanchet et al., 2008; Narisetty, 2020; Vu et al., 2015), can be employed for this purpose (Heinze et al., 2018).

In this research, we adopt a stepwise forward procedure. Theoretically, such a procedure starts with a null model (i.e., devoid of any variables), and a new variable is sequentially introduced at each step based on predefined criteria. Notably, the variable that maximizes the improvement in the chosen criterion is selected. As a result, the procedure yields a sequence of models, and the final model is selected when no significant improvement in criteria is observed.

However, the variable selection we implement does not cover the whole initial dataset of our predictors. Specifically, we do not include in this process four variables: rainfall anomaly, preparatory rainfall, slope unit area and catchment ID. The above-mentioned predictors are included as ex-officio members in our modeling. We force the presence of such variables because they play a crucial role in capturing essential aspects of the phenomenon and modeling, and their exclusion might lead to a skewed representation of the dynamics we aim to understand. As a result, our stepwise routine does not start with a null model, but with a default one including these variables.

Within this framework, we employ the *Area Under the Curve* (hereafter, AUC) as the criterion to guide the selection process from our initial set of predictors (see, Section 3.2). The AUC is associated with the *Receiver Operating Characteristic Curve*, which is constructed by plotting on the y-axis the *True Positive Rate* (TPR) or *Sensitivity*, whereas on the x-axis is reported the *False Positive Rate* (FPR) or *1-Specificity*. In our framework, the TPR corresponds to the rate of SUs correctly classified with the presence of landslides, while the FPR is the rate of SUs wrongly labeled with landslides. The AUC stands out as a widely used cut-off independent metric for evaluating the performance of binary classification models (Hosmer and Lemeshow, 2000; Hossin and Sulaiman, 2015).

To improve the model's robustness, we also take into account for spatial dependence in our selection procedure. Specifically, the variable selection procedure works in conjunction with a spatial cross-validation routine (Brenning, 2012; Meyer et al., 2018), allowing to select variables that lead to the highest spatial performance (Meyer et al., 2019). To achieve this, the *K-Means* algorithm (Lloyd, 1982; MacQueen et al., 1967) is used to group SUs into a predetermined number of clusters. In our context, we spatially divide our data into five clusters. We opt for this specific number of clusters after conducting numerous tests. Notably, it emerged as the minimum required to prevent the occurrence of clusters devoid of SUs labeled with presence of landslides. As a consequence, the impact of each variable is evaluated by fitting the associated model on four clusters and evaluating its performance on the remaining one. The process iterates until the model is tested on all clusters, with the variable contributing to the highest average AUC score being added to the subset at each step.

3.4. Performance assessment

In this section, we describe the adopted cross-validation routines to evaluate the performance of our model. Our first approach involves the implementation of a classic random cross-validation (RCV). This technique implies the division of the dataset into ten subsets. The model is then trained on nine of these subsets, constituting 90 % of the dataset, and subsequently evaluated on the remaining subset, representing 10 % of the dataset (Rodriguez et al., 2009; Wieczorek, 1984). This process is repeated iteratively until each subset serves as a test set. However, the use of a single RCV iteration may yield a somewhat noisy estimate of the model's performance. Therefore, we choose to repeat the partitioning procedure ten times, resulting in a total of 100 subsets. This iterative repetition serves to mitigate the influence of any specific random split, offering a more stable and representative evaluation of the model's overall performance (Kim, 2009). Despite the repetition of partition, a classical RCV approach may ignore the spatial dependence in the dataset leading to an overoptimistic performance estimation (Brenning, 2005; Gudmundsson and Seneviratne, 2015; Meyer et al., 2018).

As a consequence, several approaches to incorporate a spatial dependence within cross-validation procedures have been proposed (Brenning, 2012; Le Rest et al., 2014; Pohjankukka et al., 2017; Roberts et al., 2017). These methods are often referred to as spatial cross-validation (SCV) and offer dependable assessments of model performance. In short, SCV enables the examination of how the model's predictive abilities may differ across spatial areas, offering insights into its spatial robustness. Consequently, it becomes possible to identify areas associated with the worst-case scenario. In light of these considerations, we opt to build a SCV strategy to further delve into our model capabilities. The SCV strategy we develop is based on the *K-means* clustering algorithm. As for the variable selection procedure (see, Section 3.3.1), we cluster our SUs into five folds by using the x and y coordinates of their centroids. To further randomize this clustering we choose to repeat it ten times, resulting in a five-by-ten partition. As a result, we train the model over four folds and test its performance with the remaining one, and repeating this routine across all the random spatial folds for a total of 50 replicates.

Similarly to the selection of the best subset of predictors, we evaluate the model's performance in both routines through the AUC.

4. Results and discussion

In this section, we present and discuss the results of our modeling. We initially show the results of our spatial variable selection and report the best subset of predictors on which we build our EBM (Section 4.1). In Section 4.2, we examine the intelligibility of our EBM by showing the overall importance of each predictor, the global feature effects, and local explanations for individual mapping units. Subsequently, we provide a summary of the model performances resulting from the RCV and SCV routines we implement (Section 4.3). Ultimately, we describe the cartographic transposition of model outputs (Section 4.4).

4.1. Spatial variable selection

In Fig. 3, we present the outcomes of the variable selection process. The x-axis displays the number of variables incorporated into our model's default configuration. In contrast, the y-axis reports the mean AUC value obtained through spatial validation for each new model configuration. A notable observation is the limited difference among the performances of various configurations. Despite this, the models consistently demonstrate average performance values below 0.70, indicating an apparent limitation in accuracy (Streiner and Cairney, 2007). However, the reason behind this trend is primarily attributable to the spatial distribution of SUs labeled with landslides. The implications of this distribution on AUC computation are discussed in Section 4.3.

Notably, the mean AUC values resulting from spatial cross-validations show a marginal discrepancy of 0.01 A closer analysis reveals an ascending trend in AUC scores up to the sixth addition to the default model configuration. Subsequent iterations do not display any noticeable increase or decrease, leading to the identification of the sixth iteration as the optimal model configuration.

As a result, our final set of predictors is constituted by ten variables: rainfall anomaly, preparatory rainfall, slope unit area, catchment ID, standard deviation of slope, soil type, land cover, lithology, catchment slope angle, and contributing area. This selected set includes the variables that collectively contribute to the highest average spatial impact on model performances. For instance, one can notice the absence of the mean slope steepness among the final set of predictors. The spatial selection highlights the limited influence of this variable on the model's predictive capabilities. The homogeneity in mean slope steepness values across all SUs precludes its utility as a discriminatory predictor for distinguishing SUs with landslides from those without. Conversely, the standard deviation of slope steepness results as the first variable added to the default configuration. This is not surprising, as similar outcomes are reported also in other studies (Canavesi et al., 2020). This outcome is consistent with earlier considerations regarding slope steepness: the standard deviation captures better than the mean value the variability and the peculiarity of the geomorphological features of each SU. As a result, this predictor proves to be an optimal proxy for terrain roughness and demonstrates greater discriminatory capability in our specific context.

Furthermore, excluded predictors include northness, eastness, TWI, SPI, and several types of curvatures. Despite being conventional variables in landslide susceptibility modeling (Fang et al., 2023; Goetz et al., 2015; Marjanović et al., 2011), these parameters show negligible spatial influence in our case study. For instance, TWI is valuable in assessing general terrain wetness and moisture conditions (Sørensen et al., 2005). However, these indirect parameterizations become uninfluential if triggering and antecedent rainfall patterns are explicitly used as inputs to the model.

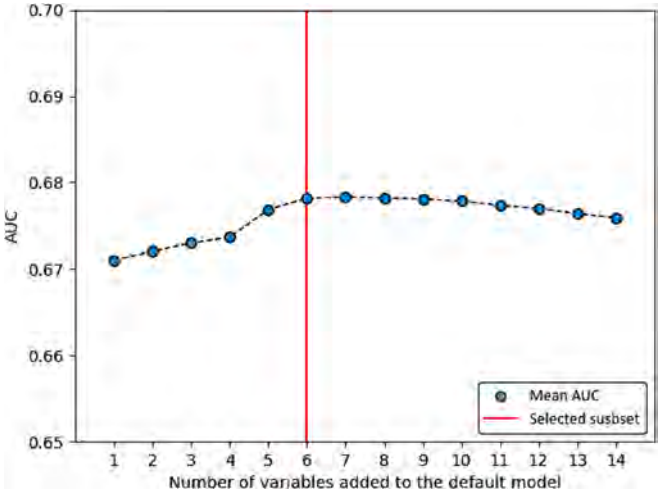

Fig. 3. Results of the spatial variable selection procedure. On the y-axis, the AUC values related to each corresponding subset of predictors are reported. The x-axis shows the number of variables within each subset.

Similarly, northness and eastness do not only express the orientation of a slope but they also acquire the relationship between orientation and soil conditions. However, their role in triggering landslides is debated and largely dependant on local climatic and morphological conditions (Nurwatik et al., 2022). Focusing on the northern hemisphere, landslides are more common in north and west-facing slopes than in the south or east-facing directions (Gritzner et al., 2001). The primary reason is related to solar radiation, north and west-facing slopes receive less direct sunlight and, consequently, tend to be shaded (Måren et al., 2015). This may result in slower evapotranspiration and lead to higher soil water content. As a result, the increased water content may reduce shear strength and contribute to slope instability. However, the exclusion of northness and eastness suggests that the spatial orientation of slopes may not significantly contribute to the landslide occurrence under such conditions. In extreme rainfall events, the intensity and duration of rainfall play a crucial role in triggering landslides (Guzzetti et al., 2008; Rosi et al., 2012; Saito et al., 2010; Segoni et al., 2014). Whether the event is exceptionally intense (as in our case), the role of slope orientation may be overshadowed. In addition, extreme events lead to rapid saturation of the soil and an increase in pore pressure in a short time. As a consequence, the role of those settings that normally control such conditions is minimized.

Therefore, these exclusions are further proof of the exceptional nature of the modeled event. Specifically, the variables included in the final set mainly represent conditions related to the triggering event, such as rainfall anomaly and preparatory rainfall, as well as predisposing factors. Among these latter, the presence of contributing area and catchment slope angle allows for capturing the terrain response to extreme rainfall, offering a more targeted and contextually relevant landslide susceptibility modeling under such conditions. In short, the final set is closely tied to the dynamics of extreme rainfall-induced landslides, ensuring a more tailored and effective representation of the susceptibility factors in our specific modeling context.

4.2. Model interpretability

In this section, we show the direct intelligibility of our model by reporting the overall importances, the global and local effects of landslide predictors.

Fig. 4 displays the importance of each variable within our modeling framework. The importance quantification is achieved through a mean absolute score, as determined by the application of Eq. (4). In short, this absolute score provides a metric for the average impact of each independent variable on the final estimation (see, Section 3.3). Upon analyzing the overall impacts, it is evident that rainfall anomaly emerges as the most important variable. This observation suggests that the model distinctly recognizes the dominant influence of rainfall event dynamics on landslide occurrence. Notably, slope unit area, lithology, the pairwise interaction between rainfall anomaly and preparatory rainfall, as well as catchment ID, show notable high absolute scores. Conversely, the variable of land cover turns out to be the least significant in terms of importance.

Specifically, the presence of slope unit area among variables with higher scores suggests its ability to capture a potential mapping-related bias within our modeling framework.

In Fig. 5, we present an overview of the estimated variable effects, which are expressed at the scale of logits. We opt to show them at this scale instead of the response scale due to its preferable interpretability for the analysis of individual variable contributions. However, the information is essentially the same between the logit and response scales. Specifically, a negative score means that the response (i.e., susceptibility

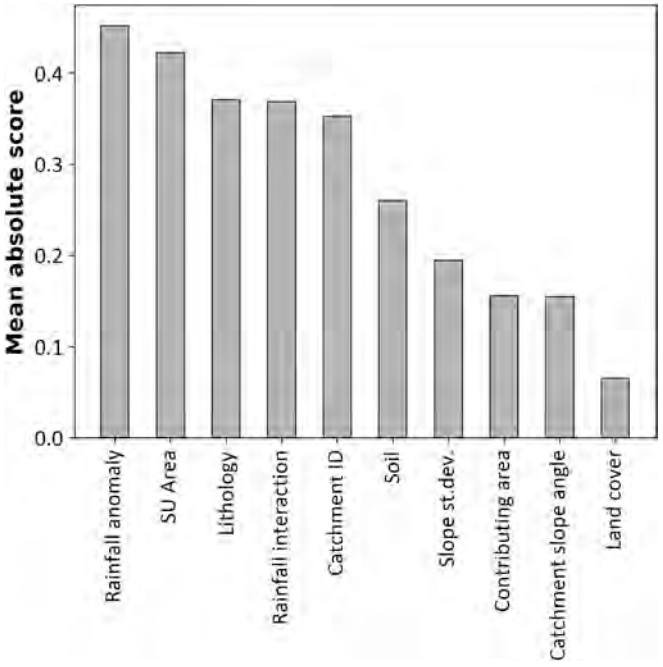

Fig. 4. Summary of predictor's importances. The importances are expressed via a mean absolute score. Rainfall interaction means the pairwise interaction term between preparatory rainfall and rainfall anomaly.

estimate) tends to decrease suggesting in our context more stable conditions. Conversely, a positive contribution indicates an increase in the susceptibility, hence a greater likelihood of landslide occurrence.

Going back to the overall effects, we notice that the standard deviation of slope steepness (Fig. 5A) shows a negative influence up to a threshold of 4°. Beyond this threshold, a positive trend is linearly reported. A possible justification for this pattern lies in the fact that a rougher terrain denotes a more juvenile landscape where geomorphic processes tend to be more intense and frequent (Glenn et al., 2006; Helming et al., 1998). As a consequence, this soil may be more susceptible to destabilization during an extreme rainfall event.

In Fig. 5B and C, the contributions of logarithmic contributing area and corresponding average slope angle are reported. These are initially included in our set of predictors to capture effects related to soil moisture and destabilizing force upslope. Both shape functions show some artifacts due to the absence of values in specific intervals. The low data density contributes to a significant variability of effects, evident in the larger grey bands within these regions. An example of this is observed into the influence associated with a logarithmic contributing area greater than 7 (corresponding to 10 km^2). By delving into the impact of the upslope contributing area, one can notice an increasing trend between the interval corresponding to 10,000 m^2 and 100,000 m^2. During this range, the effect transitions from negative to positive scores. A plausible explanation for this influence is that soil saturation is more likely to occur in larger contributing areas. In these areas, the accumulation of water from various sources, such as precipitation and upstream flow, may be more substantial (Montgomery and Dietrich, 1994). As a result, the soil is rapidly saturated and the slope stability may be compromised under the increased moisture content.

The catchment slope angle shows a negative influence up to 11°, after which we observe a positive contribution to landslide occurrence. From a geomorphic perspective, the observation is reasonable since steeper upslope areas may be destabilized due to overloading (Brenning et al., 2015). This overload can lead to increased stress and reduced stability, contributing to conditions conducive to landslides.

Overall, the standard deviation of slope steepness, the logarithmic upslope contributing area, and the catchment slope angle do not report positive effects overtaking a threshold of 0.5. This means they have a weak influence on the landslide occurrence in our context. Notably, they are included in the last four variables in terms of importance. These results point out that the landslide occurrence we model is mainly driven by triggering factors rather than geomorphological settings. The effects of additional predisposing conditions—specifically lithology, land cover, and soil type—are displayed in panels D, E, and F of Fig. 5 respectively. The lithological class with the most significant positive influence on our susceptibility estimates is *Lit7*, which corresponds to flysch. These sedimentary rocks consist of alternating layers of hard, resistant rocks, and softer ones. Notably, the presence of weaker layers within the flysch sequence is usually associated to potential slip planes for landslides (Azañón et al., 2010; Borgatti et al., 2006). In case of their saturation, the clayey layers can lose their strength, leading to failure and sliding. Given the rapid rates at which saturation can occur during

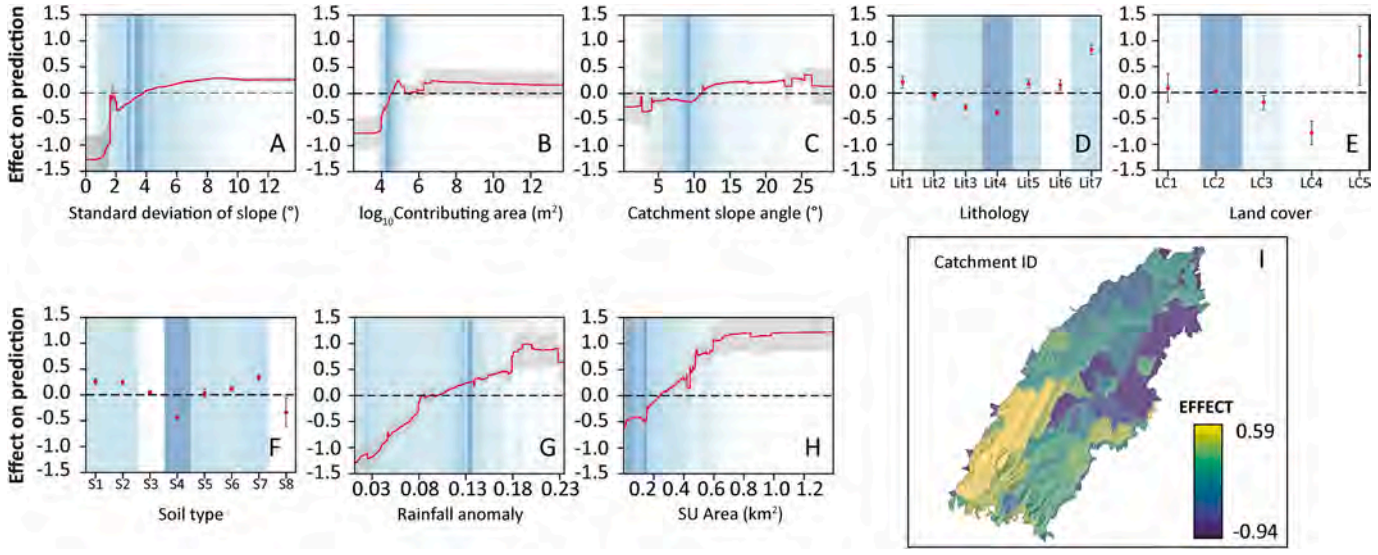

Fig. 5. Overview of the single effects of variables. The effects on prediction are represented in logits. Continuous variables (Panels A, B, C, G, H) display mean effects with red lines and 95 % confidence intervals with grey bands. Categorical variables (Panels D, E, F) depict mean effects with red circles and 95 % confidence intervals with grey error bars. Note that dark blue regions indicate high data density, whereas white areas signify low densities. Panel I reports the corresponding effect of each catchment. The corresponding classes of lithology, land cover, and soil type are described in Tables S1, S2 and S3, respectively.

extreme rainfall events, the estimated effect aligns logically with our study context.

Looking at the contribution of land cover classes (Fig. 5E), one can notice that class *LC5* shows both the highest positive influence and larger variability. This class represents open spaces with little or no vegetation across our study area. A possible justification for its effect may be found in the role of vegetation on slope stability. Specifically, vegetation helps in stabilizing soil and preventing erosion. The root systems of plants bind soil particles together, reducing the likelihood of slope failure (Masi et al., 2021). In open spaces with little or no vegetation, there is less reinforcement of soil structure, making the area more susceptible to landslides. On the contrary, the scrub class (*LC4)* displays the most negative effect on landslide occurrence. Different from open spaces, scrub lands may have strong root systems that contribute to soil stability.

In Fig. 5F, the effects associated with soil typologies are depicted. One can notice that several typologies provide weak positive influences on landslide occurrence. Conversely, the most popular class *S4*-calcaric regosols- shows the most negative estimated effect. A plausible explanation for this trend may lie in their role in human activities. In our study area, the calcaric regosols are mainly associated with lands assigned to agricultural practices that involve terracing. Such activities may improve the stability and contribute to decreasing the likelihood of landslide occurrence. On the contrary, the S7 – hypocalcic calcisols class reports the highest influence on landslide occurrence. This relationship has been already observed in other contexts of the Italian Apennines. Specifically, the reason may lie in the presence of a harder, less permeable horizon rich in carbonate concretions at depth. This layer allows rainwater to accumulate during intense rainstorms, which increases pore-water pressure leading to slope failure (Bordoni et al., 2021a).

The effect associated with the rainfall anomaly is depicted in Fig. 5G. We recall that this variable is computed to capture the intensity of the rainfall event of September 15, 2022, in relation to past rainfall patterns. The estimated influence shows an almost linear trend, as the rainfall anomaly increases, so does the impact. The rainfall anomaly effect can be further divided into three distinct sectors. In the range of the rainfall anomaly from 0.03 to approximately 0.08, the effect increases, although it remains negative. This trend highlights moderate rainfall intensities that do not represent a relevant trigger for the analyzed landscape. Beyond 0.08, the influence shows a shift to neutral and then positive scores, steadily increasing until reaching the threshold of 0.18. This tendency suggests that increasing levels of extreme rainfalls are anomalous compared to typical climatic conditions of the study area, thus representing a relevant trigger for new landslides. Subsequently, there is another significant jump in scores, resulting in a highly positive influence on landslide occurrence. Specifically, after the 0.18 value an increase in rainfall anomaly does not directly translate into an increase in susceptibility. The reason may lie in the fact that after a given threshold value of rainfall is exceeded, all possible landslides would have been triggered. It's important to note that this phenomenon is primarily associated with low data densities for values within the mentioned range of rainfall anomalies. As a consequence, the variability in this range is more pronounced compared to the earlier trends. Overall, the spatial pattern of rainfall anomalies controls the spatial occurrence of landslides.

The effect of interaction between rainfall anomaly and preparatory rainfall is displayed In Fig. 6. We recall that the preparatory rainfall expresses the cumulative precipitation over the 30 days before the analyzed rainfall event. By examining this joint effect, noteworthy instances of positive impact emerge. Specifically, positive scores are observed when both rainfall anomaly and preparatory rainfall reach their peak values. However, these scores show considerable variability due to the limited data densities associated with high values of both rainfall parameters. Furthermore, a substantial positive effect is discerned when the rainfall anomaly falls within the range of 0.025 to

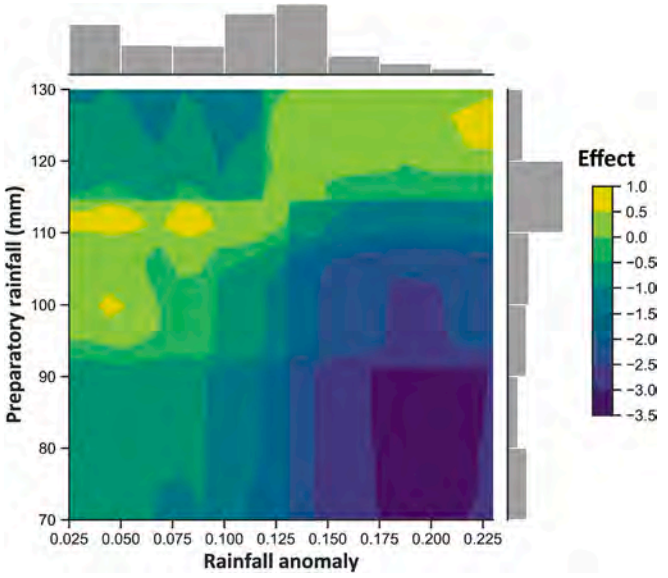

Fig. 6. Summary of the effect associated with the pairwise interaction between rainfall anomaly and preparatory rainfall. The histograms on the upper axis show the distribution of rainfall anomaly intervals. Conversely, the histograms on the right axis display the distribution of corresponding preparatory rainfall intervals.

approximately 0.100, with preparatory rainfall close to 110 mm. Delving into the interaction within the region of the highest data density for both rainfall anomaly and preparatory rainfall also reveals a positive influence on landslide occurrence. Conversely, the most negative effect is shown when rainfall anomalies exceed 0.175 and preparatory rainfall is less than 90 mm. Although this trend may appear somewhat counterintuitive, considering the expectation of a positive influence for the highest values of rainfall anomaly, it is plausible to interpret it as a suggestion that the overall effect of event intensity is amplified by specific antecedent conditions. However, it should be noted that such an occurrence does not happen in our context. By analyzing the SUs reporting a rainfall anomaly greater than 0.175, we notice that they show a minimum preparatory rainfall of 118 mm. As a consequence, this particular case is characterized by a notable degree of uncertainty.

The variable slope unit area exhibits a relatively continuous increasing trend, as depicted in Fig. 5H. By analyzing this effect, it becomes evident that SUs with larger areas tend to have a higher influence to landslide occurrence. At first glance, one might infer a direct correlation: the larger the SU, the higher the estimated landslide susceptibility. However, such an interpretation is misleading, as the areal extent of a mapping unit does not inherently influence slope stability. To address this potential bias, we have incorporated a procedure for bias capture and removal within our analysis. This step enables the model to isolate the areal contribution, ensuring that it does not directly propagate its impact on our landslide susceptibility scores (Moreno et al., 2024). By excluding this effect, our analysis aims to avoid any ambiguity in predictions associated with the choice of mapping units.

The same analytical steps are applied to the variable catchment ID (Fig. 5I). This variable is incorporated into our model to account for spatial relationships among slope units (SUs). However, the catchment ID itself does not directly influence the likelihood of slope failure. Therefore, the model incorporates its effect and subsequently, we exclude it during the prediction phase.

As outlined in Section 3.3, EBMs offer the capability to visualize the local effects of variables. In short, the model explains its decision-making process for each prediction. By leveraging this capability, it is possible to analyze how each variable influences the estimated susceptibility score. For brevity, we present a concise overview of this

interpretability aspect for three distinct cases (Fig. 7). A local explanation for a SU for which the model predicts a final susceptibility estimate close to 0 is depicted in Fig. 7A. Among all variables, land cover emerges as the unique contributor with a positive influence on the susceptibility estimate. However, this influence is nearly negligible, compared to the impact of other predictors. Conversely, all other predictors exhibit negative scores, leading the model to predict a very low susceptibility value for the examined SU. Notably, rainfall variables show the most significant influences among all predictors.

In Fig. 7B, we display a scenario where the final susceptibility score is 0.50. This implies a condition halfway between an unstable and stable slope. One can notice that the effects of the predictors seem to offset each other to some extent.

Ultimately, we provide an overview of an SU in Fig. 7C, where the model predicts a very high susceptibility score. In this case, only one variable, the catchment slope angle, has a negative impact on the model output. Conversely, the remaining predictors demonstrate positive influences, with rainfall components showing the most substantial contribution.

4.3. Model performances

Here, we show the results of the two cross-validation routines we implement to assess the performances of our model. We recall that the routines are based respectively on a random (RCV) and spatial (SCV) partition of our dataset.

The outcomes resulting from the 100-fold RCV are depicted in Fig. 8. Looking at the AUC score for the reference model reveals a value of 0.87, which indicates an excellent classifier according to Hosmer and Lemeshow (2000). Similarly, the scores resulting from the 100-fold RCV routine highlight the optimal classification capabilities of our model. Specifically, this routine shows a mean AUC of 0.86, which is close to the score of the reference model. The marginal discrepancy observed between these performance metrics suggests an inherent robustness of the model. By analyzing in depth the 100 performances resulting from the random partition, we notice the associated AUC scores exhibit a variability of 0.03, expressed as a single standard deviation. Notably, the worst scenario is represented by an AUC of 0.78, whereas the best scenario achieves an AUC of 0.92. This range further confirms the robustness and classification capabilities of our model.

However, using a RCV scheme may occasionally result in an overoptimistic representation of model capabilities. This is because a random split might yield a favorable partition that aligns well with the model fit. In short, the associated performances may not accurately reflect the model's true generalization ability to unseen data. To both delve into the performances of our model and evaluate it on unknown regions, we implement a 50-fold SCV (see, Section 3.4).

Fig. 9 displays the results of such a routine through a cartographic

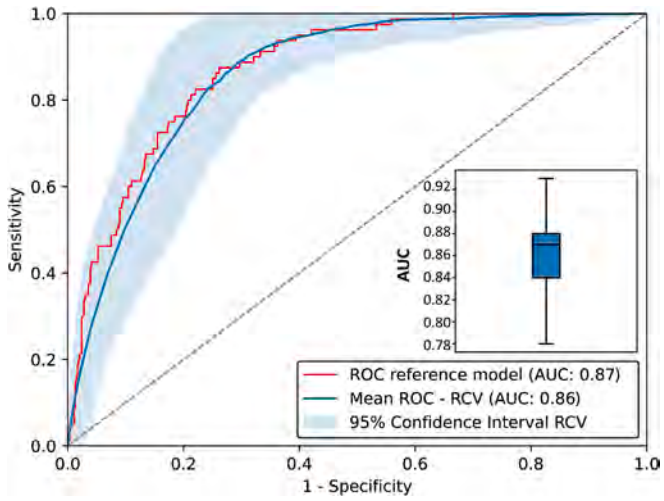

Fig. 8. Summary of the 100-fold RCV. The average ROC curve resulting from the routine is displayed with the associated confidence interval. The ROC curve of the reference model is represented by the red curve. The boxplot shows the distribution of the AUC values resulting from the RCV routine.

representation. Specifically, we visualize for each partition the spatial distribution of associated AUC scores and the number of SUs labeled with landslides via a bivariate scheme. This allows us to recognize the relationship between the adopted evaluation metric and the number of true positive cases. Notably, the AUC values are grouped into three classes following the classification scheme proposed by Hosmer and Lemeshow (2000), whereas the number of SUs with landslides is classified through the Jenks method (Jenks and Caspall, 1971; North, 2009). Overall, the outcomes of the SCV scheme report AUC scores ranging from 0.50 to 0.94, hence spanning from a random classifier to an excellent one. This information is captured by a mean value of 0.60 and a standard deviation of 0.10, which indicates a higher variability compared to that observed in the RCV procedure. Specifically, the reported mean value may suggest a weakness in our model. However, these data might be misleading by looking at the overall context displayed in Fig. 9. Notably, each clustering iteration shows several worst-case scenarios of performance (grey and blue clusters). In particular, the areas where the model struggles to accurately predict landslide occurrence are situated in both the southern and northern sectors of the study area. There are numerous reasons behind these poor predictive capabilities. In the case of the southern sectors, the main justification is the huge amount of SUs hosting landslides within their domains. Going back to Fig. 2A, one can notice that these regions encompass the majority of mapped landslides. Therefore, when they serve as validation clusters, the model fit is devoid of an enormous quantity of landslide information.

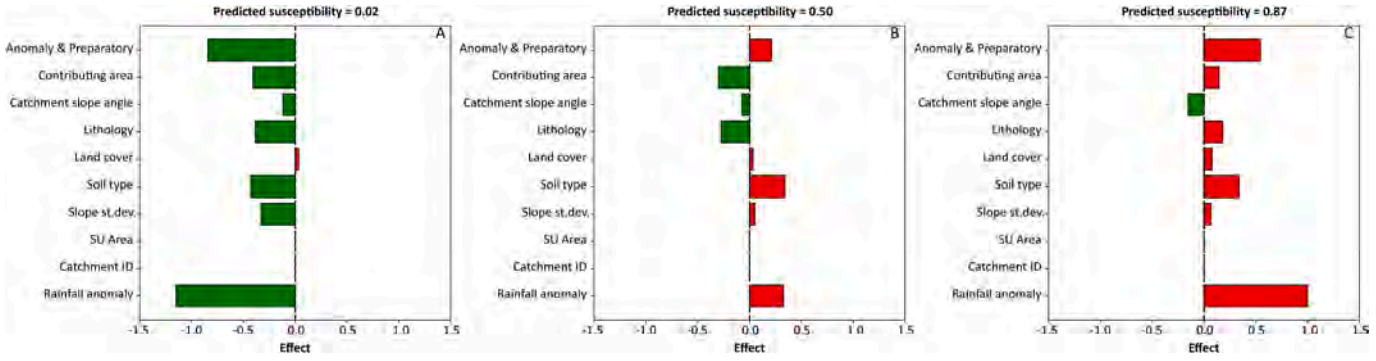

Fig. 7. Examples of local explanations for three different predicted susceptibility scores. The x-axis shows the associated local effects of each predictor, a rightward-directed effect (red bars) means a positive impact on landslide occurrence. Conversely, a leftward-directed one (green bars) indicates a negative impact. It is noteworthy that the effects of slope unit area and catchment ID are always zero because they are zeroed during prediction.

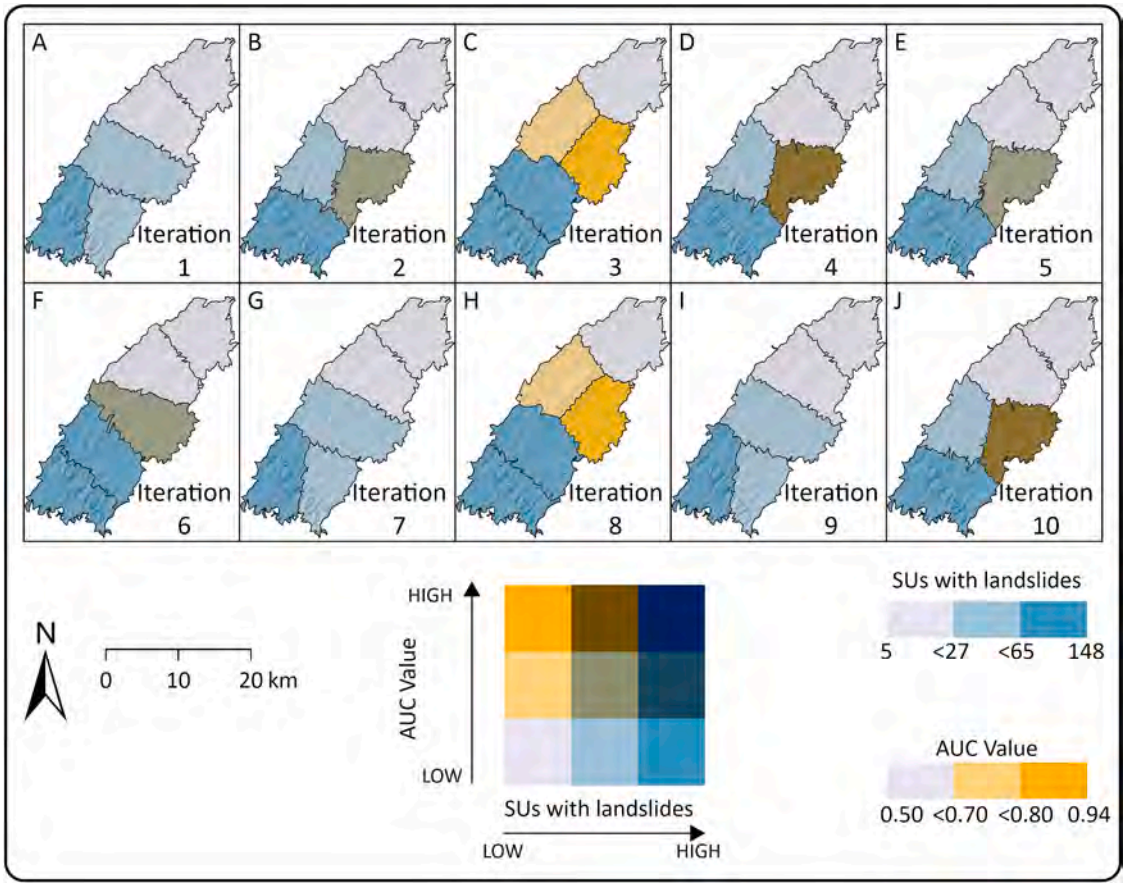

Fig. 9. Summary of the 50-fold SCV procedure. The clusters of each partition are visualized through a bivariate scheme in which the associated AUC values and number of SUs with landslides are compared.

As a consequence, the model is not capable of learning the prevailing conditions that contribute to slope instability. The incomplete understanding of such conditions leads the model to fail in predicting these occurrences. For instance, this case is represented by iteration 9 (Fig. 9I), where the blue cluster contains 58 % of SUs labeled with landslides. As verification of this observation, one can notice that no cluster classified with the highest class of number of SUs with landslides provides medium or high AUC values.

Conversely, the poor quality of prediction in the northern clusters may be associated with the scarce quantity of SUs with landslide presence. For instance, in iteration 1 (Fig. 9A) the northernmost sector reports only five SUs with landslides, which corresponds to 1.2 % of mapping units within their domains. As a result, the scarcity of these instances affects the ROC curve and the associated AUC. Notably, this highly unbalanced proportion means that the model might be inclined towards predicting the majority class (absence of landslides). As a consequence, the performances may report a high true negative rate (*Specificity*) but a low true positive rate, resulting in a low AUC.

Another explanation for this trend in the northern regions may be associated with the dynamics of the rainfall event. By referring to the rainfall anomaly, we notice that the intensity of the event in such regions is low (Fig. 10A), with the majority of the values concentrated around the threshold of 0.02 (Fig. 10B). Specifically, going back to the global effect of rainfall anomaly (Fig. 5G), it is clear that the observed anomaly values show markedly negative contributions to landslide occurrence. As a result, the presence of landslides in the northernmost sectors may elude the majority of learned model relationships, leading to model failure in this particular region. In short, while the model may capture predominant patterns between landslide presence and predisposing or triggering factors, it fails to account for outlier events that do not adhere

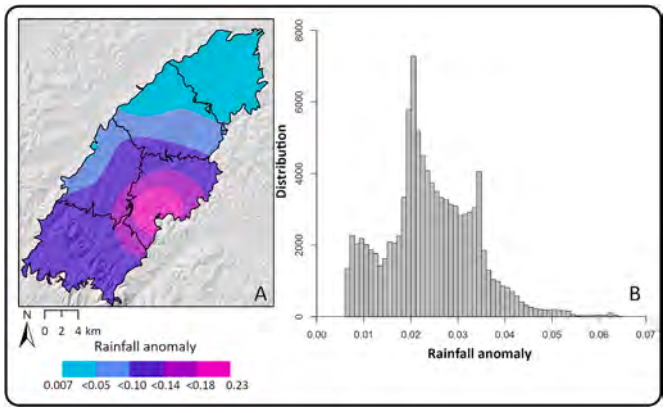

Fig. 10. Panel A shows the spatial distribution of rainfall anomaly across the study area. The example clustering partition is derived from iteration 5 in Fig. 9E. Panel B reports the distribution of rainfall anomaly values within the northernmost cluster.

to these learned relationships. Consequently, the model's predictive efficacy diminishes in scenarios where landslides occur in unexpected areas.

A further justification of the drop in model performances can be attributable to the bias removal step we include within our protocol. Notably, the removal of bias captured by the effect of slope unit area, which significantly influences model predictions on average (Fig. 4), may result in a deterioration of accuracy. However, this procedural step is essential for generating more reliable products, even though it may

entail an apparent reduction in predictive skills (Steger et al., 2021).

Conversely, the SCV scheme reveals multiple instances where the model exhibits medium to high AUC scores. These occurrences are specifically linked to conditions where the model effectively comprehends the relationship between predictors and landslide occurrences, while also being able to validate itself in regions with a substantial presence of landslides. Notably, this is exemplified in cases observed during both iteration 3 (Fig. 9C) and iteration 10 (Fig. 9J), where the model reaches excellent AUC scores.

Overall, the SCV routine seems to provide more biased estimates of model accuracy rather than the RCV approach. The pessimistic results of SCV are probably caused by strongly distinct conditions in the test areas compared to the training ones, suggesting a thorough underestimation of model capabilities.

4.4. Model results

After presenting the intelligibility and predictive capabilities of our model, we proceed to illustrate the cartographic representation of its results. The probabilistic map generated by our modeling is displayed in Fig. 11. Specifically, we opt to represent the susceptibility scores along a continuous spectrum, rather than categorizing them into distinct susceptibility levels. As a consequence, the susceptibility estimates range from 0 to 1.

By analyzing the spatial distribution of susceptibility scores, a clear trend emerges, indicating that SUs with a higher likelihood of experiencing landslides are mainly situated in the southern-western regions. From a geomorphic perspective, this spatial correlation seems reasonable given that these SUs are positioned within the most mountainous sector of the study area (see, Fig. 2A). Therefore, it is plausible to attribute this pattern to the joint influence of predisposing factors and the rainfall event, creating conditions conducive to landslide occurrences. Conversely, areas characterized by susceptibility probabilities closer to zero are primarily concentrated in the northern sector. In these regions, the rainfall anomaly shows the lowest values (see, Fig. 10), whereas the geomorphological context is less pronounced to promote landslide.

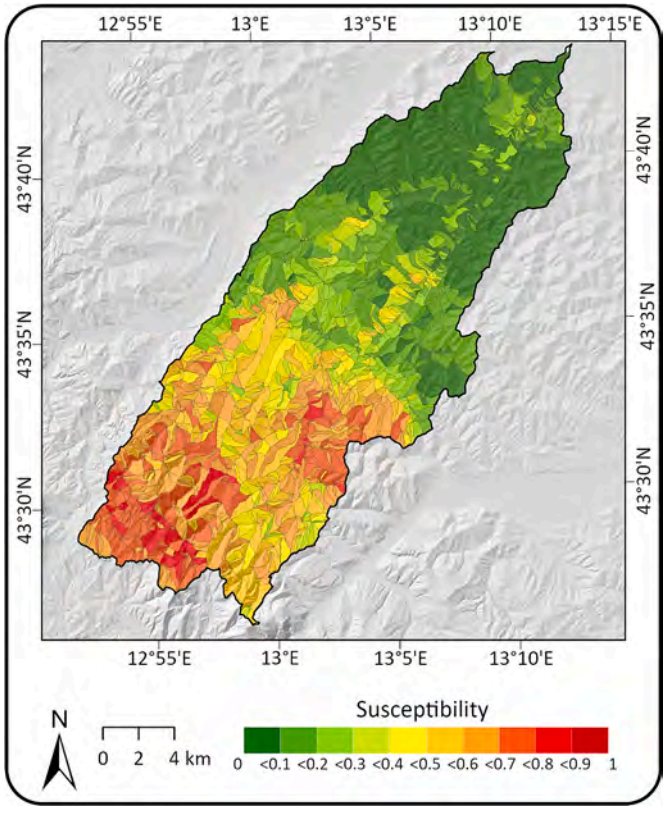

Fig. 11. Landslide susceptibility map.

Overall, the spatial arrangement of susceptibility scores appears to closely mirror the patterns observed in the rainfall anomaly. Specifically, regions that received highly anomalous rainfall amounts during the 15 September event show higher susceptibility probabilities. On the contrary, areas marked by lower intensities of rainfall events display generally lower susceptibility estimates. The observed correlation between the spatial distribution of susceptibility values and the rainfall anomaly pattern is a direct consequence of the objective of our work: in modeling landslide susceptibility based on a single extreme rainfall event, we introduce triggering factors among the input variables and we develop a model that adequately replicates reality by leveraging both environmental features and rainfall. This poses the basis for possible application of the same model, in the same area, simulating the effect of different rainfall scenarios.

4.4.1. What if the rainfall anomaly changes?

In this section, we delve into the interplay between the likelihood of landslide occurrence and the intensity of rainfall event, extending beyond the modeling of a past event to explore potential scenarios by varying the rainfall anomaly. Notably, the calculation of rainfall anomaly introduces a dynamic dimension to our model configuration, as contrarily to all other parameters used by the model, the rainfall anomaly received by each SU may vary at every future rainfall event. By leveraging this aspect, we extend our model protocol to two distinct scenarios: one where the rainfall anomaly is uniformly set at 0.08 and a second scenario defined by a rainfall anomaly equal to 0.18. We use these two values for our test because they are the values corresponding to the first and second sharp increment in the rainfall-susceptibility relationship (see, Fig. 5G).

Fig. 12 shows landslide susceptibility maps under varied rainfall anomaly scenarios. The residuals (i.e. the difference in susceptibility scores from the starting susceptibility estimates portrayed in Fig. 11) are also shown in Fig. 12A' and B'. Negative values (blue colors) suggest that the starting probabilities exceed those of the new scenarios, indicating a reduction in susceptibility. Conversely, positive scores (red colors) indicate an increase in the likelihood of landslide occurrence, highlighting that the new scores are greater than the initial ones. As a result, one can notice that differences in susceptibility estimates are directly related to changes in rainfall anomaly values. For instance, the southern SUs in Fig. 12A show lower probabilities since the initial scores are modeled with higher rainfall anomalies, hence a more positive influence on the final response. This concept is even more amplified in residuals resulting from probabilities modeled with a rainfall anomaly equal to 0.18 (Fig. 12B'). Notably, the outcomes of this configuration show a widespread increase in probabilities within the almost entire study area. One can notice that the maximum growth is registered in northern areas, reaching a peak of 0.6 in the scores.

The differences between the scenarios in Fig. 12A' and B' are summarized in Fig. 12C. Specifically, the two curves show comparable and symmetrical distributions. The curve corresponding to the scenario with a rainfall anomaly equal to 0.08 (light-blue curve) demonstrates a leftward orientation, while the curve associated with the extreme anomaly conditions (light-red curve) reports a rightward direction. These observations imply that the less extreme scenario may depict a condition more closely aligned with ordinary circumstances, whereas the more extreme scenario represents conditions considerably deviating from the normality.

4.5. Considerations: strengths and weaknesses

In this section, we provide an overview of the strengths of our analytical protocol as well as the weaknesses that came to light.

Our modeling leveraged the direct intelligibility of EBMs to inspect

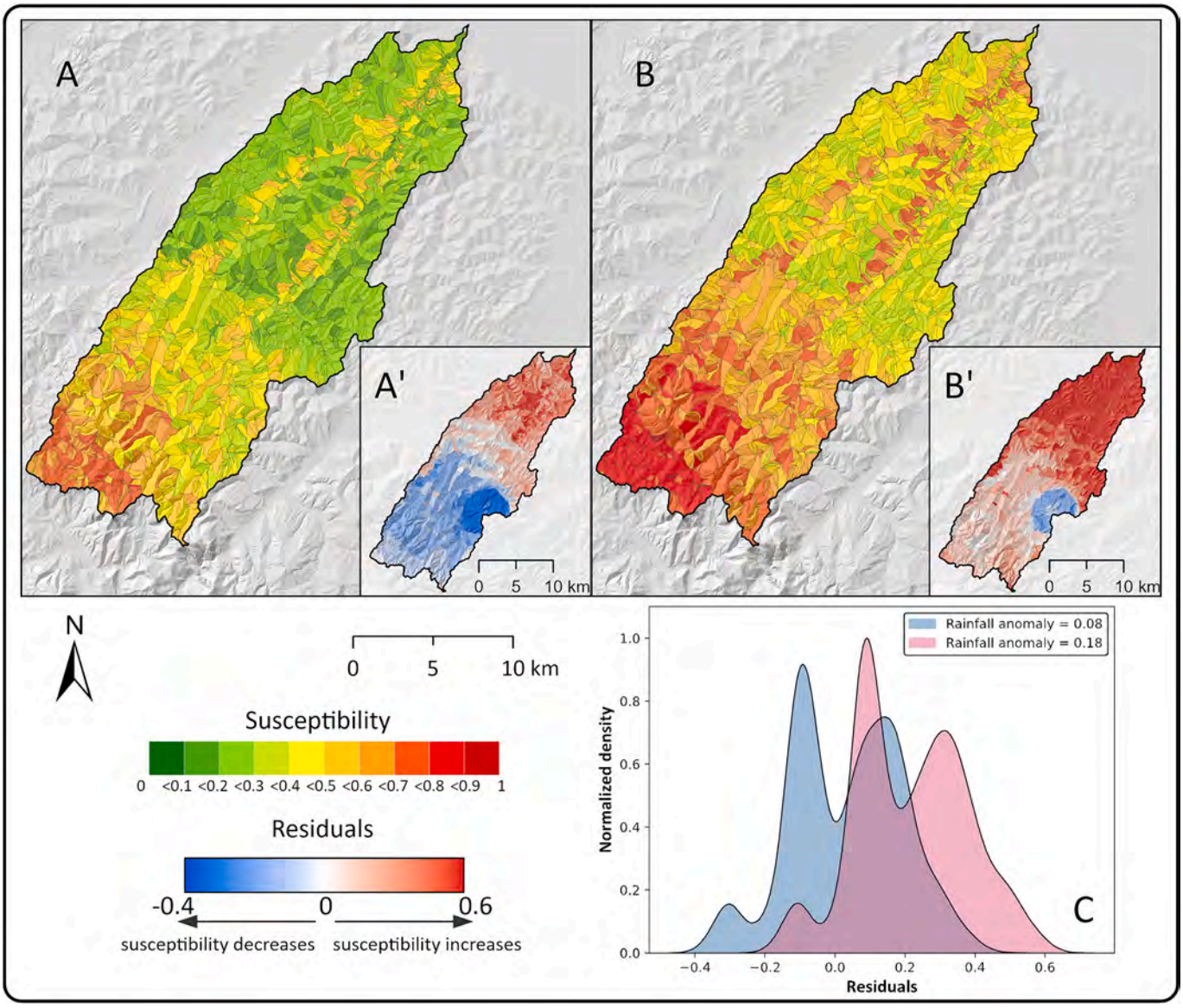

Fig. 12. Overview of landslide susceptibility values under varied rainfall anomaly scenarios. Panel A displays the landslide susceptibility scores resulting from the scenario with rainfall anomaly set to 0.08. Panel A' depicts the spatial distribution of residuals resulting from the comparison between the above-mentioned susceptibility scores and the starting susceptibility estimates (Fig. 11). Panel B reports the landslide susceptibility scores modeled with a rainfall anomaly equal to 0.18. Panel B′ showcases the corresponding residual distribution. Panel C compares the distribution of the two residuals' scenarios.

the relationship between landslide occurrence and extreme rainfall events. The inherent "transparency" in our modeling approach facilitated the extrapolation of the impact of event intensity, expressed as rainfall anomaly, on the probability of landslide occurrences throughout the study area. The contribution of rainfall anomaly (see, Fig. 5G) aligns well with the concept of rainfall thresholds for landslide occurrence (see, Segoni et al., 2018). By delving into this effect, we can identify potential thresholds that may hold the key to defining preliminary warning levels in our study area. For instance, when anticipating rainfall at 8 % of the average annual precipitation, a landslide probability close to 0.5 emerges, which may indicate a moderate warning level. Conversely, a rainfall exceeding 18 % annually corresponds to a probability of 0.73, signaling a high warning level. The affinities with rainfall thresholds may be extended even to the pairwise interaction we introduced among rainfall parameters. Notably, rainfall thresholds can be also defined considering antecedent rainfall conditions (Glade et al., 2000; Lee et al., 2015; Nocentini et al., 2023a). As a consequence, our joint effect of rainfall parameters may serve as a further tool for delineating warning levels. This observation aligns well with the growing number of studies suggesting close interoperability between susceptibility modeling and dynamic rainfall parameters (Khan et al., 2022; Lee et al., 2022; Nocentini et al., 2023b; Ren et al., 2024; Segoni et al., 2015).

The insights provided by our analytical protocol extend to the local level, specifically scrutinizing the decision-making process for estimating landslide susceptibility within individual SU. Specifically, every SU can be analyzed to understand which factors are more convenient to be addressed by mitigation measures to reduce landslide hazard (Dahal and Lombardo, 2023; Wang et al., 2024a). Fig. 7C shows an instructive example, allowing for a detailed examination of how each predictor shapes the predicted susceptibility score for the relevant SU. In this hypothetical scenario, the primary drivers influencing the probability of landslide occurrence turn out to be the rainfall parameters. As a result, the outcomes may suggest the implementation of a drainage system or reforestation measures to facilitate water flow, thereby mitigating the probability of soil saturation and erosion—factors that could otherwise contribute to the initiation of landslides. Overall, this process can be

systematically extended to all SUs. By doing so, one can identify the most critical predisposing conditions to landslides, set priorities to design mitigation measures and evaluate the cost/benefit of different intervention strategies.

Another novelty introduced by our study lies in the rainfall parameters we leverage as landslide predictors. Differently from the majority of landslide susceptibility studies, where the meteorological component is expressed by the mean yearly or monthly rainfall value (Chen and Li, 2020; Xing et al., 2021), we opt to distinguish it into event-based and antecedent conditions. As a result, we introduce a dynamic component within our modeling, which differentiates it from traditional landslide susceptibility models. Specifically, this aspect allows for producing predictions on different rainfall scenarios as discussed in Section 4.4.1. This dynamic capability proves to be a powerful asset in the context of landslide studies considering the current scenario of climate change (Araújo et al., 2022; Ozturk et al., 2022), where the incidence of extreme weather events is on the rise (AghaKouchak et al., 2020). In light of these considerations, the ability to predict landslide occurrence under different scenarios becomes particularly significant. This can be achieved by configuring new rainfall parameter values, either by extrapolating them from future projections or utilizing short-term weather forecast data. Consequently, our findings expand their utility beyond predictive modeling. In fact, they may be leveraged to produce preliminary warning levels in a cartographic format, predicting the likelihood of landslide occurrence based on different rainfall data. For instance, our modeling can be easily updated by using near-real-time rainfall data, hence it may provide a useful product for communication on landslide threats.

Despite its inherent dynamic nature, our modeling currently focuses solely on predicting the probability of landslide occurrence in a spatial dimension. This is because our model analyzes relationships between landslide events and predictors based on single-event conditions. Notably, our model currently examines the influence of extreme rainfall conditions on landslide occurrence. While this spatial analysis provides valuable insights, a constraint arises from the absence of temporal information in the Italian Landslide Inventory (Trigila et al., 2010). The absence of temporal data presents a limitation, impeding the implementation of a more detailed approach. Ideally, incorporating temporal data into our modeling framework may enable a comprehensive space-time analysis of landslide occurrence (Fang et al., 2024; Lombardo et al., 2020; Nocentini et al., 2023b). This approach could capture both predisposing and triggering conditions of landslides on a temporal basis, allowing for a finer examination of factors evolving over months or years. Such a space-time modeling approach may facilitate a deeper understanding of the intricate interplay of factors over time. This modeling configuration may also represent an improvement to current procedures, which treat the spatial and temporal probabilities of occurrence separately due to the assumption that they are uncorrelated (Bordoni et al., 2021b; Park et al., 2019). In this perspective, future studies could explore how certain predisposing conditions influence susceptibility over a time interval. Additionally, it could help our protocol to model ordinary conditions that currently are excluded from our analysis due to the lack of temporal information on previous landslides.

5. Conclusion

In this contribution, we explored the capabilities of a new generation of explainable machine-learning models to analyze relationships between landslide occurrence and extreme rainfall events. Leveraging the context of landslides induced by an extreme rainfall event (September 15, 2022) in the Misa River basin, we introduced a novel variable, rainfall anomaly, to express the magnitude of the reference rainfall event in our susceptibility modeling and to allow further assessment of response to different rainfall scenarios.

Our analysis revealed that rainfall anomaly emerged as the most crucial variable influencing landslide occurrence. The exact intelligibility of our modeling allowed for a comprehensive understanding of its contribution in the modeled event to landslide occurrence in comparison to other predictors. The introduction of rainfall anomaly also brought a dynamic facet to our protocol, enabling the estimation of landslide susceptibility under varying rainfall scenarios. This adaptability is particularly significant in the context of increasing extreme events due to climate change as it allows modeling the response of territory (in terms of ground effects to hypothetical or forecasted future rainfall scenarios.

Our procedure represents a promising step that could be strengthened in the future as long as the effects of the next extreme rainfall events are considered to broaden the calibration. Indeed, at present our modeling relies solely on information from the analyzed event, lacking temporal details from previously mapped landslides. Such data would have allowed for the implementation of space-time predictive analysis and modeling the landslide occurrence on both a spatial and temporal basis. Furthermore, this approach would have captured ordinary conditions that currently are excluded from our analysis.

In light of these considerations, a bunch of future improvements can be already listed. A refined modeling of rainfall scenarios, especially in its spatial distribution, may lead to a more detailed mapping of landslide susceptibility under different climatic conditions. The incorporation of temporal information on previous landslides would refine our modeling, encompassing both extreme and ordinary conditions. Covering the whole spectrum of possible triggering conditions could contribute to a more comprehensive landslide hazard assessment. A complete landslide hazard evaluation demands not only spatial and temporal probability estimation but also intensity assessment. Although spatiotemporal probabilities can be defined using a more detailed landslide inventory with temporal information, landslide intensity may be evaluated through various means, such as modeling the landslide area (Moreno et al., 2023) or considering the number of events (Di Napoli et al., 2023) per SU.

Aside from these aspects, our findings may represent a useful product for master planning and communication on possible landslide threats.

CRediT authorship contribution statement

Francesco Caleca: Writing – original draft, Visualization, Validation, Software, Methodology, Investigation, Formal analysis, Data curation, Conceptualization. **Pierluigi Confuorto:** Writing – review & editing, Visualization, Validation, Supervision, Methodology, Investigation, Formal analysis, Data curation, Conceptualization. **Federico Raspini:** Writing – review & editing, Validation, Supervision, Conceptualization. **Samuele Segoni:** Writing – review & editing, Validation, Supervision, Methodology, Conceptualization. **Veronica Tofani:** Writing – review & editing, Validation, Supervision, Methodology, Conceptualization. **Nicola Casagli:** Writing – review & editing, Supervision, Resources. **Sandro Moretti:** Writing – review & editing, Supervision, Resources.

Declaration of competing interest

The authors declare that they have no known competing financial interests or personal relationships that could have appeared to influence the work reported in this paper.

Data availability

The data and the code for this research are available at the following GitHub repository https://github.com/fcaleca1/landslide_susceptibility_EBM.

Acknowledgements

The publication was made by a researcher with a research contract

co-funded by the European Union - PON Research and Innovation 2014–2020 in accordance with Article 24, paragraph 3a), of Law No. 240 of December 30, 2010, as amended and Ministerial Decree No. 1062 of August 10, 2021.

The authors kindly acknowledge Alessia Schiaroli and Pierpaolo Tiberi (Regione Marche – Direzione Protezione Civile e Sicurezza del Territorio) for providing and sharing useful information.

Appendix A. Supplementary data

Supplementary data to this article can be found online at https://doi.org/10.1016/j.scitotenv.2024.175277.

References

AghaKouchak, A., Chiang, F., Huning, L.S., Love, C.A., Mallakpour, I., Mazdiyasni, O., Moftakhari, H., Papalexiou, S.M., Ragno, E., Sadegh, M., 2020. Climate extremes and compound hazards in a warming world. Annu. Rev. Earth Planet. Sci. 48, 519–548.
Alvioli, M., Guzzetti, F., Rossi, M., 2014. Scaling properties of rainfall induced landslides predicted by a physically based model. Geomorphology 213, 38–47.
Alvioli, M., Marchesini, I., Reichenbach, P., Rossi, M., Ardizzone, F., Fiorucci, F., Guzzetti, F., 2016. Automatic delineation of geomorphological slope units with r. slopeunits v1. 0 and their optimization for landslide susceptibility modeling. Geosci. Model Dev. 9, 3975–3991.
Amato, G., Eisank, C., Castro-Camilo, D., Lombardo, L., 2019. Accounting for covariate distributions in slope-unit-based landslide susceptibility models. A case study in the alpine environment. Eng. Geol. 260, 105237.
Amato, G., Fiorucci, M., Martino, S., Lombardo, L., Palombi, L., 2023. Earthquake-triggered landslide susceptibility in Italy by means of Artificial Neural Network. Bull. Eng. Geol. Environ. 82, 160.
Arabameri, A., Chandra Pal, S., Rezaie, F., Chakrabortty, R., Saha, A., Blaschke, T., Di Napoli, M., Ghorbanzadeh, O., Thi Ngo, P.T., 2022. Decision tree based ensemble machine learning approaches for landslide susceptibility mapping. Geocarto Int. 37, 4594–4627.
Araújo, J.R., Ramos, A.M., Soares, P.M., Melo, R., Oliveira, S.C., Trigo, R.M., 2022. Impact of extreme rainfall events on landslide activity in Portugal under climate change scenarios. Landslides 19, 2279–2293.
Ayalew, L., Yamagishi, H., 2005. The application of GIS-based logistic regression for landslide susceptibility mapping in the Kakuda-Yahiko Mountains, Central Japan. Geomorphology 65, 15–31.
Azañón, J.M., Azor, A., Yesares, J., Tsige, M., Mateos, R.M., Nieto, F., Delgado, J., López-Chicano, M., Martín, W., Rodríguez-Fernández, J., 2010. Regional-scale high-plasticity clay-bearing formation as controlling factor on landslides in Southeast Spain. Geomorphology 120, 26–37.
Azarafza, M., Azarafza, M., Akgün, H., Atkinson, P.M., Derakhshani, R., 2021. Deep learning-based landslide susceptibility mapping. Sci. Rep. 11, 24112.
Ba, Q., Chen, Y., Deng, S., Yang, J., Li, H., 2018. A comparison of slope units and grid cells as mapping units for landslide susceptibility assessment. Earth Sci. Inf. 11, 373–388.
Barlow, M., Gutowski, W.J., Gyakum, J.R., Katz, R.W., Lim, Y.-K., Schumacher, R.S., Wehner, M.F., Agel, L., Bosilovich, M., Collow, A., et al., 2019. North American extreme precipitation events and related large-scale meteorological patterns: a review of statistical methods, dynamics, modeling, and trends. Clim. Dyn. 53, 6835–6875.
Barredo, J., Benavides, A., Hervás, J., van Westen, C.J., 2000. Comparing heuristic landslide hazard assessment techniques using GIS in the Tirajana basin, Gran Canaria Island, Spain. Int. J. Appl. Earth Obs. Geoinf. 2 (1), 9–23.
Bartolini, C., 2003. When did the Northern Apennine become a mountain chain. Quat. Int. 101, 75–80.
Baryannis, G., Dani, S., Antoniou, G., 2019. Predicting supply chain risks using machine learning: the trade-off between performance and interpretability. Futur. Gener. Comput. Syst. 101, 993–1004.
Bendel, R.B., Afifi, A.A., 1977. Comparison of stopping rules in forward “stepwise” regression. J. Am. Stat. Assoc. 72, 46–53.
Beven, K.J., Kirkby, M.J., 1979. A physically based, variable contributing area model of basin hydrology/un modèle à base physique de zone d’appel variable de l’hydrologie du bassin versant. Hydrol. Sci. J. 24, 43–69.
Blanchet, F.G., Legendre, P., Borcard, D., 2008. Forward selection of explanatory variables. Ecology 89, 2623–2632.
Bogaard, T.A., Greco, R., 2016. Landslide hydrology: from hydrology to pore pressure. Wiley Interdiscip. Rev. Water 3, 439–459.
Bordoni, M., Bittelli, M., Valentino, R., Vivaldi, V., Meisina, C., 2021a. Observations on soil-atmosphere interactions after long-term monitoring at two sample sites subjected to shallow landslides. Bull. Eng. Geol. Environ. 80 (10), 7467–7491.
Bordoni, M., Vivaldi, V., Lucchelli, L., Ciabatta, L., Brocca, L., Galve, J., Meisina, C., 2021b. Development of a data-driven model for spatial and temporal shallow landslide probability of occurrence at catchment scale. Landslides 18, 1209–1229.
Borgatti, L., Corsini, A., Barbieri, M., Sartini, G., Truffelli, G., Caputo, G., Puglisi, C., 2006. Large reactivated landslides in weak rock masses: a case study from the Northern Apennines (Italy). Landslides 3, 115–124.
Bossard, M., Feranec, J., Otahel, J., 2000. CORINE Land Cover Technical Guide: Addendum 2000 (No. 40). European Environment Agency, Copenhagen.
Brabb, E.E., 1984. Innovative approaches to landslide hazard and risk mapping. In: International Landslide Symposium Proceedings, Toronto, Canada, 1, pp. 17–22.
Brenning, A., 2005. Spatial prediction models for landslide hazards: review, comparison and evaluation. Nat. Hazards Earth Syst. Sci. 5, 853–862.
Brenning, A., 2008. Statistical geocomputing combining R and SAGA: the example of landslide susceptibility analysis with generalized additive models. In: Hamburger Beiträge zur Physischen Geographie und Landschaftsökologie, 19 (23–32), p. 410.
Brenning, A., 2012. Spatial cross-validation and bootstrap for the assessment of prediction rules in remote sensing: the R package sperrorest. In: 2012 IEEE International Geoscience and Remote Sensing Symposium, pp. 5372–5375.
Brenning, A., Trombotto, D., 2006. Logistic regression modeling of rock glacier and glacier distribution: topographic and climatic controls in the semi-arid Andes. Geomorphology 81, 141–154.
Brenning, A., Schwinn, M., Ruiz-Páez, A., Muenchow, J., 2015. Landslide susceptibility near highways is increased by 1 order of magnitude in the Andes of southern Ecuador, Loja province. Nat. Hazards Earth Syst. Sci. 15, 45–57.
Bucci, F., Santangelo, M., Fongo, L., Alvioli, M., Cardinali, M., Melelli, L., Marchesini, I., 2022. A new digital lithological map of Italy at the 1: 100 000 scale for geomechanical modelling. Earth Syst. Sci. Data 14, 4129–4151.
Budimir, M., Atkinson, P., Lewis, H., 2015. A systematic review of landslide probability mapping using logistic regression. Landslides 12, 419–436.
Bui, D.T., Tsangaratos, P., Nguyen, V.-T., Van Liem, N., Trinh, P.T., 2020. Comparing the prediction performance of a Deep Learning Neural Network model with conventional machine learning models in landslide susceptibility assessment. Catena 188, 104426.
Calderoni, G., Della Seta, M., Fredi, P., Lupia Palmieri, E., Nesci, O., Savelli, D., Troiani, F., et al., 2010. Late Quaternary geomorphological evolution of the Adriatic coast reach encompassing the Metauro, Cesano and Misa river mouths (Northern Marche, Italy). Geo Acta Spec. Publ. 3, 109–124.
Caleca, F., Tofani, V., Segoni, S., Raspini, F., Rosi, A., Natali, M., Catani, F., Casagli, N., 2022. A methodological approach of QRA for slow-moving landslides at a regional scale. Landslides 19, 1539–1561.
Camilo, D.C., Lombardo, L., Mai, P.M., Dou, J., Huser, R., 2017. Handling high predictor dimensionality in slope-unit-based landslide susceptibility models through LASSO-penalized Generalized Linear Model. Environ. Model Softw. 97, 145–156.
Campbell, R.H., 1973. Isopleth map of landslide deposits, Point Dume Quadrangle, Los Angeles County, California; an experiment in generalizing and quantifying areal distribution of landslides. In: Technical Report. US Geological Survey.
Canavesi, V., Segoni, S., Rosi, A., Ting, X., Nery, T., Catani, F., Casagli, N., 2020. Different approaches to use morphometric attributes in landslide susceptibility mapping based on meso-scale spatial units: a case study in Rio de Janeiro (Brazil). Remote Sens. 12, 1826.
Carrara, A., 1983. Multivariate models for landslide hazard evaluation. J. Int. Assoc. Math. Geol. 15, 403–426.
Carrara, A., Merenda, L., 1976. Landslide inventory in northern Calabria, southern Italy. Geol. Soc. Am. Bull. 87, 1153–1162.
Carrara, A., Cardinali, M., Detti, R., Guzzetti, F., Pasqui, V., Reichenbach, P., 1991. GIS techniques and statistical models in evaluating landslide hazard. Earth Surf. Process. Landf. 16, 427–445.
Caruana, R., Lundberg, S., Ribeiro, M.T., Nori, H., Jenkins, S., 2020. Intelligible and explainable machine learning: best practices and practical challenges. In: Proceedings of the 26th ACM SIGKDD International Conference on Knowledge Discovery & Data Mining, pp. 3511–3512.
Catani, F., Lagomarsino, D., Segoni, S., Tofani, V., 2013. Landslide susceptibility estimation by random forests technique: sensitivity and scaling issues. Nat. Hazards Earth Syst. Sci. 13, 2815–2831.
Centamore, E., Chiocchini, U., Cipriani, N., Deiana, G., Micarelli, A., 1979. The minor basins in the context of the Umbro-Marchean region tectonic-sedimentary evolution during Middle-Upper Miocene. In: Ann. Geol. Pays Hellen, Tome Hors Serie, pp. 247–251.
Centamore, E., Ciccacci, S., Del Monte, M., Fredi, P., Palmieri, E.L., 1996. Morphological and morphometric approach to the study of the structural arrangement of northeastern Abruzzo (central Italy). Geomorphology 16, 127–137.
Chang, Z., Catani, F., Huang, F., Liu, G., Meena, S.R., Huang, J., Zhou, C., 2023. Landslide susceptibility prediction using slope unit-based machine learning models considering the heterogeneity of conditioning factors. J. Rock Mech. Geotech. Eng. 15, 1127–1143.
Chen, W., Li, Y., 2020. GIS-based evaluation of landslide susceptibility using hybrid computational intelligence models. Catena 195, 104777.
Clò, S., David, F., Segoni, S., 2024. The impact of hydrogeological events on firms: evidence from Italy. J. Environ. Econ. Manag. 124, 102942.
Collini, E., Palesi, L.A.I., Nesi, P., Pantaleo, G., Nocentini, N., Rosi, A., 2022. Predicting and understanding landslide events with explainable AI. IEEE Access 10, 31175–31189.
Coltori, M., 1997. Human impact in the Holocene fluvial and coastal evolution of the Marche region, Central Italy. Catena 30, 311–335.
Conforti, M., Ietto, F., 2021. Modeling shallow landslide susceptibility and assessment of the relative importance of predisposing factors, through a GIS-based statistical analysis. Geosciences 11 (8), 333.
Corominas, J., van Westen, C., Frattini, P., Cascini, L., Malet, J.-P., Fotopoulou, S., Catani, F., Van Den Eeckhaut, M., Mavrouli, O., Agliardi, F., et al., 2014. Recommendations for the quantitative analysis of landslide risk. Bull. Eng. Geol. Environ. 73, 209–263.
Crozier, M.J., 2010. Deciphering the effect of climate change on landslide activity: a review. Geomorphology 124, 260–267.

Dahal, A., Lombardo, L., 2023. Explainable artificial intelligence in geoscience: a glimpse into the future of landslide susceptibility modeling. Comput. Geosci. 176, 105364.
Dayan, U., Nissen, K., Ulbrich, U., 2015. Atmospheric conditions inducing extreme precipitation over the eastern and western Mediterranean. Nat. Hazards Earth Syst. Sci. 15, 2525–2544.
Deckers, J.A., Nachtergaele, F., 1998. World Reference Base for Soil Resources: Introduction, Vol. 1. Acco Publishers, Leuven, pp. 81–84.
Di Napoli, M., Tanyas, H., Castro-Camilo, D., Calcaterra, D., Cevasco, A., Di Martire, D., Pepe, G., Brandolini, P., Lombardo, L., 2023. On the estimation of landslide intensity, hazard and density via data-driven models. Nat. Hazards 119, 1513–1530.
Erener, A., Düzgün, H., 2012. Landslide susceptibility assessment: what are the effects of mapping unit and mapping method? Environ. Earth Sci. 66, 859–877.
Ermini, L., Catani, F., Casagli, N., 2005. Artificial neural networks applied to landslide susceptibility assessment. Geomorphology 66, 327–343.
Fang, Z., Wang, Y., van Westen, C., Lombardo, L., 2023. Space–time landslide susceptibility modeling based on data-driven methods. Math. Geosci. 1–20.
Fang, Z., Wang, Y., van Westen, C., Lombardo, L., 2024. Landslide hazard spatiotemporal prediction based on data-driven models: estimating where, when and how large landslide may be. Int. J. Appl. Earth Obs. Geoinf. 126, 103631.
Gameiro, S., Riffel, E.S., de Oliveira, G.G., Guasselli, L.A., 2021. Artificial neural networks applied to landslide susceptibility: the effect of sampling areas on model capacity for generalization and extrapolation. Appl. Geogr. 137, 102598.
Gariano, S.L., Guzzetti, F., 2016. Landslides in a changing climate. Earth Sci. Rev. 162, 227–252.
Gatto, A., Clò, S., Martellozzo, F., Segoni, S., 2023. Tracking a decade of hydrogeological emergencies in Italian municipalities. Data 8, 151.
Giles, P.T., Franklin, S.E., 1998. An automated approach to the classification of the slope units using digital data. Geomorphology 21, 251–264.
Glade, T., Crozier, M.J., 2005. The nature of landslide hazard impact. In: Landslide Hazard and Risk, pp. 41–74.
Glade, T., Crozier, M., Smith, P., 2000. Applying probability determination to refine landslide-triggering rainfall thresholds using an empirical "Antecedent Daily Rainfall Model". Pure Appl. Geophys. 157, 1059–1079.
Glenn, N.F., Streutker, D.R., Chadwick, D.J., Thackray, G.D., Dorsch, S.J., 2006. Analysis of LiDAR-derived topographic information for characterizing and differentiating landslide morphology and activity. Geomorphology 73, 131–148.
Goetz, J., Brenning, A., Petschko, H., Leopold, P., 2015. Evaluating machine learning and statistical prediction techniques for landslide susceptibility modeling. Comput. Geosci. 81, 1–11.
Goetz, J.N., Guthrie, R.H., Brenning, A., 2011. Integrating physical and empirical landslide susceptibility models using generalized additive models. Geomorphology 129, 376–386.
Greenwell, B.M., Dahlmann, A., Dhoble, S., 2023. Explainable Boosting Machines with Sparsity – Maintaining Explainability in High-dimensional Settings.
Gritzner, M.L., Marcus, W.A., Aspinall, R., Custer, S.G., 2001. Assessing landslide potential using GIS, soil wetness modeling and topographic attributes, Payette River, Idaho. Geomorphology 37, 149–165.
Gudmundsson, L., Seneviratne, S.I., 2015. Towards observation-based gridded runoff estimates for Europe. Hydrol. Earth Syst. Sci. 19, 2859–2879.
Guzzetti, F., 2005. Landslide hazard and risk assessment (PhD thesis). Universitäts-und Landesbibliothek Bonn.
Guzzetti, F., Carrara, A., Cardinali, M., Reichenbach, P., 1999. Landslide hazard evaluation: a review of current techniques and their application in a multi-scale study, Central Italy. Geomorphology 31, 181–216.
Guzzetti, F., Reichenbach, P., Cardinali, M., Galli, M., Ardizzone, F., 2005. Probabilistic landslide hazard assessment at the basin scale. Geomorphology 72, 272–299.
Guzzetti, F., Reichenbach, P., Ardizzone, F., Cardinali, M., Galli, M., 2006. Estimating the quality of landslide susceptibility models. Geomorphology 81, 166–184.
Guzzetti, F., Peruccacci, S., Rossi, M., Stark, C.P., 2008. The rainfall intensity–duration control of shallow landslides and debris flows: an update. Landslides 5, 3–17.
Guzzetti, F., Mondini, A.C., Cardinali, M., Fiorucci, F., Santangelo, M., Chang, K.-T., 2012. Landslide inventory maps: new tools for an old problem. Earth Sci. Rev. 112, 42–66.
Hansen, A., Franks, C., Kirk, P., Brimicombe, A., Tung, F., 1995. Application of GIS to hazard assessment, with particular reference to landslides in Hong Kong. In: Geographical Information Systems in Assessing Natural Hazards, pp. 273–298.
Haque, U., Da Silva, P.F., Devoli, G., Pilz, J., Zhao, B., Khaloua, A., Wilopo, W., Andersen, P., Lu, P., Lee, J., et al., 2019. The human cost of global warming: deadly landslides and their triggers (1995–2014). Sci. Total Environ. 682, 673–684.
Hastie, T., Tibshirani, R., 1987. Generalized additive models: some applications. J. Am. Stat. Assoc. 82, 371–386.
Heerdegen, R.G., Beran, M.A., 1982. Quantifying source areas through land surface curvature and shape. J. Hydrol. 57, 359–373.
Heinze, G., Wallisch, C., Dunkler, D., 2018. Variable selection–a review and recommendations for the practicing statistician. Biom. J. 60, 431–449.
Helming, K., Römkens, M., Prasad, Sn, 1998. Surface roughness related processes of runoff and soil loss: a flume study. Soil Sci. Soc. Am. J. 62, 243–250.
Hoerl, A.E., Kennard, R.W., 1970. Ridge regression: applications to nonorthogonal problems. Technometrics 12, 69–82.
Hosmer, D.W., Lemeshow, S., 2000. Applied Logistic Regression, Vol. 398. John Wiley & Sons.
Hossin, M., Sulaiman, M.N., 2015. A review on evaluation metrics for data classification evaluations. Int. J. Data Min. Knowl. Manag. Process 5 (2), 1.
Huang, F., Zhang, J., Zhou, C., Wang, Y., Huang, J., Zhu, L., 2020. A deep learning algorithm using a fully connected sparse autoencoder neural network for landslide susceptibility prediction. Landslides 17, 217–229.
Huang, Y., Zhao, L., 2018. Review on landslide susceptibility mapping using support vector machines. Catena 165, 520–529.
Intrieri, E., Gigli, G., Mugnai, F., Fanti, R., Casagli, N., 2012. Design and implementation of a landslide early warning system. Eng. Geol. 147, 124–136.
Jacinth Jennifer, J., Saravanan, S., 2021. Artificial neural network and sensitivity analysis in the landslide susceptibility mapping of Idukki district, India. Geocarto Int. 37 (19), 5693–5715.
Jacobs, L., Kervyn, M., Reichenbach, P., Rossi, M., Marchesini, I., Alvioli, M., Dewitte, O., 2020. Regional susceptibility assessments with heterogeneous landslide information: slope unit-vs. pixel-based approach. Geomorphology 356, 107084.
Jenks, G.F., Caspall, F.C., 1971. Error on choroplethic maps: definition, measurement, reduction. Ann. Assoc. Am. Geogr. 61, 217–244.
Khan, S., Kirschbaum, D.B., Stanley, T.A., Amatya, P.M., Emberson, R.A., 2022. Global landslide forecasting system for hazard assessment and situational awareness. Front. Earth Sci. 10, 878996.
Kim, J.-H., 2009. Estimating classification error rate: repeated cross-validation, repeated hold-out and bootstrap. Comput. Stat. Data Anal. 53, 3735–3745.
Kirschbaum, D., Adler, R., Adler, D., Peters-Lidard, C., Huffman, G., 2012. Global distribution of extreme precipitation and high-impact landslides in 2010 relative to previous years. J. Hydrometeorol. 13, 1536–1551.
Le Rest, K., Pinaud, D., Monestiez, P., Chadoeuf, J., Bretagnolle, V., 2014. Spatial leave-one-out cross-validation for variable selection in the presence of spatial autocorrelation. Glob. Ecol. Biogeogr. 23, 811–820.
Lee, E., 2001. Geomorphological mapping. Geol. Soc. Lond. Eng. Geol. Spec. Publ. 18, 53–56.
Lee, J.-J., Song, M.-S., Yun, H.-S., Yum, S.-G., 2022. Dynamic landslide susceptibility analysis that combines rainfall period, accumulated rainfall, and geospatial information. Sci. Rep. 12, 18429.
Lee, S., 2005. Application of logistic regression model and its validation for landslide susceptibility mapping using GIS and remote sensing data. Int. J. Remote Sens. 26, 1477–1491.
Lee, S., Won, J.-S., Jeon, S.W., Park, I., Lee, M.J., 2015. Spatial landslide hazard prediction using rainfall probability and a logistic regression model. Math. Geosci. 47, 565–589.
Lima, P., Steger, S., Glade, T., Murillo-García, F.G., 2022. Literature review and bibliometric analysis on data-driven assessment of landslide susceptibility. J. Mt. Sci. 19, 1670–1698.
Lima, P., Steger, S., Glade, T., Mergili, M., 2023. Conventional data-driven landslide susceptibility models may only tell us half of the story: potential underestimation of landslide impact areas depending on the modeling design. Geomorphology 430, 108638.
Lin, Q., Lima, P., Steger, S., Glade, T., Jiang, T., Zhang, J., Liu, T., Wang, Y., 2021. National-scale data-driven rainfall induced landslide susceptibility mapping for China by accounting for incomplete landslide data. Geosci. Front. 12, 101248.
Linardatos, P., Papastefanopoulos, V., Kotsiantis, S., 2020. Explainable ai: a review of machine learning interpretability methods. Entropy 23, 18.
Liu, S., Wang, L., Zhang, W., He, Y., Pijush, S., 2023. A comprehensive review of machine learning-based methods in landslide susceptibility mapping. Geol. J. 58 (6), 2283–2301.
Lloyd, S., 1982. Least squares quantization in PCM. IEEE Trans. Inf. Theory 28, 129–137.
Loche, M., Alvioli, M., Marchesini, I., Bakka, H., Lombardo, L., 2022. Landslide susceptibility maps of Italy: lesson learnt from dealing with multiple landslide types and the uneven spatial distribution of the national inventory. Earth Sci. Rev. 232, 104125.
Lombardo, L., Mai, P.M., 2018. Presenting logistic regression-based landslide susceptibility results. Eng. Geol. 244, 14–24.
Lombardo, L., Opitz, T., Ardizzone, F., Guzzetti, F., Huser, R., 2020. Space-time landslide predictive modelling. Earth Sci. Rev. 209, 103318.
Lombardo, L., Tanyas, H., Huser, R., Guzzetti, F., Castro-Camilo, D., 2021. Landslide size matters: a new data-driven, spatial prototype. Eng. Geol. 293, 106288.
Lou, Y., Caruana, R., Gehrke, J., 2012. Intelligible models for classification and regression. In: Proceedings of the 18th ACM SIGKDD International Conference on Knowledge Discovery and Data Mining, pp. 150–158.
Lou, Y., Caruana, R., Gehrke, J., Hooker, G., 2013. Accurate intelligible models with pairwise interactions. In: Proceedings of the 19th ACM SIGKDD International Conference on Knowledge Discovery and Data Mining, KDD '13. Association for Computing Machinery, New York, NY, USA, pp. 623–631.
Lundberg, S.M., Lee, S.-I., 2017. A unified approach to interpreting model predictions. In: Advances in Neural Information Processing Systems, vol. 30. Curran Associates, Inc.
MacQueen, J., et al., 1967. Some methods for classification and analysis of multivariate observations. In: Proceedings of the Fifth Berkeley Symposium on Mathematical Statistics and Probability, 1st Series. Oakland, CA, USA, pp. 281–297.
Måren, I.E., Karki, S., Prajapati, C., Yadav, R.K., Shrestha, B.B., 2015. Facing north or south: does slope aspect impact forest stand characteristics and soil properties in a semiarid trans-Himalayan valley? J. Arid Environ. 121, 112–123.
Marengo, J.A., Alves, L.M., Ambrizzi, T., Young, A., Barreto, N.J., Ramos, A.M., 2020. Trends in extreme rainfall and hydrogeometeorological disasters in the Metropolitan Area of São Paulo: a review. Ann. N. Y. Acad. Sci. 1472, 5–20.
Marjanović, M., Kovačević, M., Bajat, B., Voženílek, V., 2011. Landslide susceptibility assessment using SVM machine learning algorithm. Eng. Geol. 123, 225–234.
Masi, E.B., Segoni, S., Tofani, V., 2021. Root reinforcement in slope stability models: a review. Geosciences 11, 212.
Maxwell, A.E., Sharma, M., Donaldson, K.A., 2021. Explainable boosting machines for slope failure spatial predictive modeling. Remote Sens. 13, 4991.

Mayer, L., Menichetti, M., Nesci, O., Savelli, D., 2003. Morphotectonic approach to the drainage analysis in the North Marche region, central Italy. Quat. Int. 101, 157–167. https://doi.org/10.1016/S1040-6182(02)00098-8.
McDonald, G.C., 2009. Ridge regression. Wiley Interdiscip. Rev. Comput. Stat. 1, 93–100.
Meijerink, A., 1988. Data acquisition and data capture through terrain mapping unit. ITC J. 1, 23–24.
Merghadi, A., Yunus, A.P., Dou, J., Whiteley, J., ThaiPham, B., Bui, D.T., Avtar, R., Abderrahmane, B., 2020. Machine learning methods for landslide susceptibility studies: a comparative overview of algorithm performance. Earth Sci. Rev. 207, 103225.
Meyer, H., Reudenbach, C., Hengl, T., Katurji, M., Nauss, T., 2018. Improving performance of spatio-temporal machine learning models using forward feature selection and target-oriented validation. Environ. Model Softw. 101, 1–9.
Meyer, H., Reudenbach, C., Wöllauer, S., Nauss, T., 2019. Importance of spatial predictor variable selection in machine learning applications–moving from data reproduction to spatial prediction. Ecol. Model. 411, 108815.
Montgomery, D.R., Dietrich, W.E., 1994. A physically based model for the topographic control on shallow landsliding. Water Resour. Res. 30, 1153–1171.
Moore, I.D., Grayson, R., Ladson, A., 1991. Digital terrain modelling: a review of hydrological, geomorphological, and biological applications. Hydrol. Process. 5, 3–30.
Moreno, M., Steger, S., Tanyas, H., Lombardo, L., 2023. Modeling the area of co-seismic landslides via data-driven models: the Kaikōura example. Eng. Geol. 320, 107121.
Moreno, M., Lombardo, L., Crespi, A., Zellner, P.J., Mair, V., Pittore, M., van Westen, C., Steger, S., 2024. Space-time data-driven modeling of precipitation-induced shallow landslides in South Tyrol, Italy. Sci. Total Environ. 912, 169166.
Murdoch, W.J., Singh, C., Kumbier, K., Abbasi-Asl, R., Yu, B., 2019. Interpretable machine learning: definitions, methods, and applications. In: arXiv Preprint arXiv: 1901.04592.
Muthukrishnan, R., Rohini, R., 2016. LASSO: a feature selection technique in predictive modeling for machine learning. In: 2016 IEEE International Conference on Advances in Computer Applications (ICACA), pp. 18–20. https://doi.org/10.1109/ICACA.2016.7887916.
Narisetty, N.N., 2020. Chapter 4 - bayesian model selection for high-dimensional data. In: Srinivasa Rao, A.S.R., Rao, C.R. (Eds.), Principles and Methods for Data Science, Handbook of Statistics. Elsevier, pp. 207–248. https://doi.org/10.1016/bs.host.2019.08.001.
Nefeslioglu, H., Sezer, E., Gokceoglu, C., Bozkir, A., Duman, T., et al., 2010. Assessment of landslide susceptibility by decision trees in the metropolitan area of Istanbul, Turkey. Math. Probl. Eng. 2010.
Nelder, J.A., Wedderburn, R.W., 1972. Generalized linear models. J. R. Stat. Soc. Ser. A: Stat. Soc. 135, 370–384.
Nocentini, N., Medici, C., Barbadori, F., Gatto, A., Franceschini, R., del Soldato, M., Rosi, A., Segoni, S., 2023a. Optimization of rainfall thresholds for landslide early warning through false alarm reduction and a multi-source validation. Landslides 1–15.
Nocentini, N., Rosi, A., Segoni, S., Fanti, R., 2023b. Towards landslide space-time forecasting through machine learning: the influence of rainfall parameters and model setting. Front. Earth Sci. 11, 1152130.
Nori, H., Jenkins, S., Koch, P., Caruana, R., 2019. InterpretML: A Unified Framework for Machine Learning Interpretability. https://doi.org/10.48550/arXiv.1909.09223.
North, M.A., 2009. A method for implementing a statistically significant number of data classes in the jenks algorithm. In: 2009 Sixth International Conference on Fuzzy Systems and Knowledge Discovery. IEEE, pp. 35–38.
Nurwatik, N., Ummah, M.H., Cahyono, A.B., Darminto, M.R., Hong, J.-H., 2022. A comparison study of landslide susceptibility spatial modeling using machine learning. ISPRS Int. J. Geo Inf. 11, 602.
Ozturk, U., Bozzolan, E., Holcombe, E.A., Shukla, R., Pianosi, F., Wagener, T., 2022. How climate change and unplanned urban sprawl bring more landslides. Nature 608, 262–265.
Park, J.Y., Lee, S.R., Lee, D.H., Kim, Y.T., Lee, J.S., 2019. A regional-scale landslide early warning methodology applying statistical and physically based approaches in sequence. Eng. Geol. 260, 105193.
Persichillo, M.G., Bordoni, M., Meisina, C., 2017. The role of land use changes in the distribution of shallow landslides. Sci. Total Environ. 574, 924–937.
Philip, G., Watson, D.F., 1982. A precise method for determining contoured surfaces. APPEA J. 22, 205–212.
Pike, R.J., 1988. The geometric signature: quantifying landslide-terrain types from digital elevation models. Math. Geol. 20, 491–511.
Pohjankukka, J., Pahikkala, T., Nevalainen, P., Heikkonen, J., 2017. Estimating the prediction performance of spatial models via spatial k-fold cross validation. Int. J. Geogr. Inf. Sci. 31, 2001–2019.
Prein, A.F., Liu, C., Ikeda, K., Trier, S.B., Rasmussen, R.M., Holland, G.J., Clark, M.P., 2017. Increased rainfall volume from future convective storms in the US. Nat. Clim. Chang. 7, 880–884.
Quinn, P., Beven, K., Chevallier, P., Planchon, O., 1991. The prediction of hillslope flow paths for distributed hydrological modelling using digital terrain models. Hydrol. Process. 5, 59–79.
Reichenbach, P., Galli, M., Cardinali, M., Guzzetti, F., Ardizzone, F., 2005. Geomorphological mapping to assess landslide risk: concepts, methods and applications in the Umbria region of central Italy. In: Landslide Hazard and Risk, pp. 429–468.
Reichenbach, P., Rossi, M., Malamud, B.D., Mihir, M., Guzzetti, F., 2018. A review of statistically-based landslide susceptibility models. Earth Sci. Rev. 180, 60–91.
Ren, T., Gao, L., Gong, W., 2024. An ensemble of dynamic rainfall index and machine learning method for spatiotemporal landslide susceptibility modeling. Landslides 21, 257–273.
Ribeiro, M.T., Singh, S., Guestrin, C., 2016. "Why should i trust you?": explaining the predictions of any classifier. In: Proceedings of the 22nd ACM SIGKDD International Conference on Knowledge Discovery and Data Mining, KDD '16. Association for Computing Machinery, New York, NY, USA, pp. 1135–1144.
Roberts, D.R., Bahn, V., Ciuti, S., Boyce, M.S., Elith, J., Guillera-Arroita, G., Hauenstein, S., Lahoz-Monfort, J.J., Schröder, B., Thuiller, W., et al., 2017. Cross-validation strategies for data with temporal, spatial, hierarchical, or phylogenetic structure. Ecography 40, 913–929.
Rodriguez, J.D., Perez, A., Lozano, J.A., 2009. Sensitivity analysis of k-fold cross validation in prediction error estimation. IEEE Trans. Pattern Anal. Mach. Intell. 32, 569–575.
Rosi, A., Segoni, S., Catani, F., Casagli, N., 2012. Statistical and environmental analyses for the definition of a regional rainfall threshold system for landslide triggering in Tuscany (Italy). J. Geogr. Sci. 22, 617–629.
Rosi, A., Frodella, W., Nocentini, N., Caleca, F., Havenith, H.B., Strom, A., Saidov, M., Bimurzaev, G.A., Tofani, V., 2023. Comprehensive landslide susceptibility map of Central Asia. Nat. Hazards Earth Syst. Sci. 23, 2229–2250.
Rossi, G., Catani, F., Leoni, L., Segoni, S., Tofani, V., 2013. HIRESSS: a physically based slope stability simulator for HPC applications. Nat. Hazards Earth Syst. Sci. 13, 151–166.
Rudin, C., 2019. Stop explaining black box machine learning models for high stakes decisions and use interpretable models instead. Nat. Mach. Intell. 1, 206–215.
Saito, H., Nakayama, D., Matsuyama, H., 2010. Relationship between the initiation of a shallow landslide and rainfall intensity—duration thresholds in Japan. Geomorphology 118, 167–175.
Salvatici, T., Tofani, V., Rossi, G., D'Ambrosio, M., Tacconi Stefanelli, C., Masi, E.B., Rosi, A., Pazzi, V., Vannocci, P., Petrolo, M., et al., 2018. Application of a physically based model to forecast shallow landslides at a regional scale. Nat. Hazards Earth Syst. Sci. 18, 1919–1935.
Schlögel, R., Marchesini, I., Alvioli, M., Reichenbach, P., Rossi, M., Malet, J.-P., 2018. Optimizing landslide susceptibility zonation: effects of DEM spatial resolution and slope unit delineation on logistic regression models. Geomorphology 301, 10–20.
Segoni, S., Rossi, G., Rosi, A., Catani, F., 2014. Landslides triggered by rainfall: a semi-automated procedure to define consistent intensity–duration thresholds. Comput. Geosci. 63, 123–131.
Segoni, S., Lagomarsino, D., Fanti, R., Moretti, S., Casagli, N., 2015. Integration of rainfall thresholds and susceptibility maps in the Emilia Romagna (Italy) regional-scale landslide warning system. Landslides 12, 773–785.
Segoni, S., Piciullo, L., Gariano, S.L., 2018. A review of the recent literature on rainfall thresholds for landslide occurrence. Landslides 15, 1483–1501.
Seta, M., Monte, M., Fredi, P., Miccadei, E., Nesci, O., Pambianchi, G., Piacentini, T., Troiani, F., 2008. Morphotectonic evolution of the Adriatic piedmont of the Apennines: an advancement in the knowledge of the Marche-Abruzzo border area. Geomorphology 102, 119–129.
Sørensen, R., Zinko, U., Seibert, J., 2005. On the calculation of the topographic wetness index: evaluation of different methods based on field observations. Hydrol. Earth Syst. Sci. 10, 101–112. https://doi.org/10.5194/HESS-10-101-2006.
Stage, A.R., 1976. An expression for the effect of aspect, slope, and habitat type on tree growth. For. Sci. 22, 457–460.
Stanley, T., Kirschbaum, D.B., 2017. A heuristic approach to global landslide susceptibility mapping. Nat. Hazards 87, 145–164.
Steger, S., Brenning, A., Bell, R., Glade, T., 2016a. The propagation of inventory-based positional errors into statistical landslide susceptibility models. Nat. Hazards Earth Syst. Sci. 16, 2729–2745.
Steger, S., Brenning, A., Bell, R., Petschko, H., Glade, T., 2016b. Exploring discrepancies between quantitative validation results and the geomorphic plausibility of statistical landslide susceptibility maps. Geomorphology 262, 8–23.
Steger, S., Brenning, A., Bell, R., Glade, T., 2017. The influence of systematically incomplete shallow landslide inventories on statistical susceptibility models and suggestions for improvements. Landslides 14, 1767–1781.
Steger, S., Mair, V., Kofler, C., Pittore, M., Zebisch, M., Schneiderbauer, S., 2021. Correlation does not imply geomorphic causation in data-driven landslide susceptibility modelling–benefits of exploring landslide data collection effects. Sci. Total Environ. 776, 145935.
Streiner, D.L., Cairney, J., 2007. What's under the ROC? An introduction to receiver operating characteristics curves. Can. J. Psychiatr. 52, 121–128.
Sun, D., Wen, H., Wang, D., Xu, J., 2020b. A random forest model of landslide susceptibility mapping based on hyperparameter optimization using Bayes algorithm. Geomorphology 362, 107201.
Sun, X., Chen, J., Han, X., Bao, Y., Zhan, J., Peng, W., 2020a. Application of a GIS-based slope unit method for landslide susceptibility mapping along the rapidly uplifting section of the upper Jinsha River, South-Western China. Bull. Eng. Geol. Environ. 79, 533–549.
Tarquini, S., Isola, I., Favalli, M., Mazzarini, F., Bisson, M., Pareschi, M.T., Boschi, E., 2007. TINITALY/01: a new triangular irregular network of Italy. Ann. Geophys. 50, 407–425.
Tarquini, S., Isola, I., Favalli, M., Battistini, A., Dotta, G., 2023. TINITALY, a Digital Elevation Model of Italy With a 10 Meters Cell Size (Version 1.1). https://doi.org/10.13127/TINITALY/1.1.
Taylor, D.W., 1948. Fundamentals of Soil Mechanics, vol. 66. LWW.
Tibshirani, R., 1996. Regression selection and shrinkage via the lasso. J. R. Stat. Soc. Ser. B 58, 267–288.

Toms, B.A., Barnes, E.A., Ebert-Uphoff, I., 2020. Physically interpretable neural networks for the geosciences: applications to earth system variability. J. Adv. Model. Earth Syst. 12.
Trigila, A., Iadanza, C., Spizzichino, D., 2010. Quality assessment of the Italian Landslide Inventory using GIS processing. Landslides 7, 455–470.
Tsukamoto, Y., Ohta, T., 1988. Runoff process on a steep forested slope. J. Hydrol. 102, 165–178.
Van Dao, D., Jaafari, A., Bayat, M., Mafi-Gholami, D., Qi, C., Moayedi, H., Van Phong, T., Ly, H.-B., Le, T.-T., Trinh, P.T., et al., 2020. A spatially explicit deep learning neural network model for the prediction of landslide susceptibility. Catena 188, 104451.
Van Rossum, G., Drake, F.L., 2009. Python 3 Reference Manual. CreateSpace, Scotts Valley, CA.
Van Rossum, G., Drake, F.L., et al., 1995. Python Reference Manual. Centrum voor Wiskunde en Informatica Amsterdam.
Vannoli, P., Basili, R., Valensise, G., 2004. New geomorphic evidence for anticlinal growth driven by blind-thrust faulting along the northern Marche coastal belt (central Italy). J. Seismol. 8, 297–312.
Vu, D.H., Muttaqi, K.M., Agalgaonkar, A.P., 2015. A variance inflation factor and backward elimination based robust regression model for forecasting monthly electricity demand using climatic variables. Appl. Energy 140, 385–394.
Wang, G., Sassa, K., 2003. Pore-pressure generation and movement of rainfall-induced landslides: effects of grain size and fine-particle content. Eng. Geol. 69, 109–125.
Wang, N., Zhang, H., Dahal, A., Cheng, W., Zhao, M., Lombardo, L., 2024a. On the use of explainable AI for susceptibility modeling: examining the spatial pattern of SHAP values. Geosci. Front. 15 (4), 101800.
Wang, T., Dahal, A., Fang, Z., van Westen, C., Yin, K., Lombardo, L., 2024b. From spatio-temporal landslide susceptibility to landslide risk forecast. Geosci. Front. 15, 101765.
Watson, D.F., 1985. A refinement of inverse distance weighted interpolation. Geo-processing 2, 315–327.
Wick, F., Kerzel, U., Feindt, M., 2020. Cyclic Boosting - an explainable supervised machine learning algorithm. In: CoRR abs/2002.03425.
Wieczorek, G.F., 1984. Preparing a detailed landslide-inventory map for hazard evaluation and reduction. Bull. Assoc. Eng. Geol. 21, 337–342.
Xia, D., Tang, H., Glade, T., Tang, C., Wang, Q., 2024. KNN-GCN: a deep learning approach for slope-unit-based landslide susceptibility mapping incorporating spatial correlations. Math. Geosci. 1–29.
Xing, X., Wu, C., Li, J., Li, X., Zhang, L., He, R., 2021. Susceptibility assessment for rainfall-induced landslides using a revised logistic regression method. Nat. Hazards 106, 97–117.
Yalcin, A., 2008. GIS-based landslide susceptibility mapping using analytical hierarchy process and bivariate statistics in Ardesen (Turkey): comparisons of results and confirmations. Catena 72, 1–12.
Yao, X., Tham, L., Dai, F., 2008. Landslide susceptibility mapping based on support vector machine: a case study on natural slopes of Hong Kong, China. Geomorphology 101, 572–582.
Youssef, K., Shao, K., Moon, S., Bouchard, L.-S., 2023. Landslide susceptibility modeling by interpretable neural network. Commun. Earth Environ. 4.
Zevenbergen, L.W., Thorne, C.R., 1987. Quantitative analysis of land surface topography. Earth Surf. Process. Landf. 12, 47–56.
Zêzere, J., Pereira, S., Melo, R., Oliveira, S., Garcia, R.A., 2017. Mapping landslide susceptibility using data-driven methods. Sci. Total Environ. 589, 250–267.
Zhang, W., He, Y., Wang, L., Liu, S., Meng, X., 2023. Landslide susceptibility mapping using random forest and extreme gradient boosting: a case study of Fengjie, Chongqing. Geol. J. 58 (6), 2372–2387.